Patron: Her Majesty The Queen

ROTHAMSTED RESEARCH

Rothamsted Research
Harpenden, Herts, AL5 2JQ

Telephone: +44 (0)1582 763133
Web: http://www.rothamsted.ac.uk/

Rothamsted Repository Download

A - Papers appearing in refereed journals

Smith, R. T. and Gilmour, D. J. 2018. The influence of exogenous organic carbon assimilation and photoperiod on the carbon and lipid metabolism of Chlamydomonas reinhardtii. *Algal Research-Biomass Biofuels and Bioproducts.* 31, pp. 122-137.

The publisher's version can be accessed at:

- https://dx.doi.org/10.1016/j.algal.2018.01.020

The output can be accessed at: https://repository.rothamsted.ac.uk/item/8477y/the-influence-of-exogenous-organic-carbon-assimilation-and-photoperiod-on-the-carbon-and-lipid-metabolism-of-chlamydomonas-reinhardtii.

© 21 February 2018, CC-BY license

17/09/2019 13:00 repository.rothamsted.ac.uk library@rothamsted.ac.uk

Rothamsted Research is a Company Limited by Guarantee
Registered Office: as above. Registered in England No. 2393175.
Registered Charity No. 802038. VAT No. 197 4201 51.
Founded in 1843 by John Bennet Lawes.

Algal Research 31 (2018) 122–137

Contents lists available at ScienceDirect

Algal Research

journal homepage: www.elsevier.com/locate/algal

The influence of exogenous organic carbon assimilation and photoperiod on the carbon and lipid metabolism of *Chlamydomonas reinhardtii*

Richard T. Smith[a,b,*], D. James Gilmour[b]

[a] Department of Plant Science, Rothamsted Research, Harpenden AL5 2JQ, United Kingdom
[b] Department of Molecular Biology and Biotechnology, University of Sheffield, Western Bank, Sheffield S10 2TN, United Kingdom

A B S T R A C T

Microalgae are a promising platform for the production of renewable fuels and oleochemicals. Despite significant research efforts to understand the mechanisms of algal lipid accumulation, the influence of commercially relevant growth conditions on the lipid metabolism is poorly understood. To characterise the impact of differing organic carbon availabilities and photoperiod on the response of the model alga *Chlamydomonas reinhardtii* to nitrogen stress, the expression of key genes involved in the central carbon metabolism were monitored over a time-course of nitrogen deprivation. In addition, the growth, PSII integrity, chlorophyll content, triacylglycerol (TAG) content, starch content, and fatty acid composition were characterised. Results indicate that both organic carbon availability and photoperiod regulate the lipid accumulation response of *C. reinhardtii*. Under mixotrophic conditions, organic carbon uptake is favoured over photosynthesis, transcript abundance of lipid synthesis genes rapidly increase and acetate is funnelled to TAG synthesis. In contrast, autotrophic cultures lacking organic carbon experienced a slower rate of photosynthetic degradation and funnelled the majority of sequestered carbon to starch synthesis. Dark periods induced catabolism of both starch and TAG in autotrophic cultures but TAG alone in mixotrophic cultures. Furthermore, diurnal light enhanced starch synthesis under mixotrophic conditions. Finally, transcript analysis indicated that *PGD1,* important for the routing of oleic acid to TAG, was reliant on organic carbon availability, resulting in reduced C18:1 fatty acid accumulation in autotrophic cultures.

1. Introduction

Nitrogen deprivation elicits a stress response in microalgae resulting in a rapid and global metabolic shift which, typically, leads to the accumulation of carbon storage molecules such as the biofuel feedstock triacylglycerol (TAG) [1]. While it is known that N deprivation causes a TAG accumulation response in the majority of algal species, the specific metabolic changes involved in this shift are relatively poorly understood; thus limiting the potential of metabolic engineering to improve TAG productivity [2]. In recent years, the development of a highly annotated genome [3,4] and specific molecular biology tools have enabled *C. reinhardtii* to emerge as an important reference species for improving the understanding of lipid accumulation. Furthermore, technological advances and reduced costs have enabled high-throughput genome-wide transcriptomic [5,6], proteomic [7,8] and metabolomic [9] investigations, providing a more comprehensive outlook of metabolic change.

Recent metabolic studies have focused almost exclusively on *C. reinhardtii* under idealised laboratory conditions of both mixotrophy and continuous light [1,6,7,10–15]. Under these conditions, upon N deprivation, genes for nitrogen transporters are immediately upregulated, quickly (< 1 h) followed by a metabolic shift to a N 'reuse and recycle' phase [1]. This phase results in a cessation of growth, chlorosis, and the degradation of high abundance N-rich molecules, such as ribosomes (particularly plastid ribosomal proteins), RuBisCo, and other abundant photosynthesis related proteins [1,14,16,17]. This photosynthetic degradation is matched with a shift towards less N intensive mitochondrial respiratory energy generation, fuelled by exogenous carbon [1,7,15]. Concurrently, cells begin to upregulate starch and TAG synthesis pathways leading to a redirection of carbon away from protein synthesis towards energy dense carbon storage molecule accumulation [12].

Carbon availability has been shown to be a vital component to lipid accumulation under nitrogen stress. Acetate is thought to be transported into the cell via a monocarboxylate transporter; 5 putative acetate permeases have been identified but have yet to characterised [12]. Intracellular acetate can be converted to acetyl-CoA through two alternative processes involving acetyl-CoA synthase (ACS) or the two-

* Corresponding author at: Current address, Department of Plant Science, Rothamsted Research, Harpenden AL5 2JQ, United Kingdom
E-mail addresses: Richard.smith@rothamsted.ac.uk (R.T. Smith), D.j.gilmour@sheffield.ac.uk (D.J. Gilmour).

https://doi.org/10.1016/j.algal.2018.01.020
Received 30 May 2017; Received in revised form 29 January 2018; Accepted 30 January 2018
Available online 21 February 2018
2211-9264/ © 2018 The Authors. Published by Elsevier B.V. This is an open access article under the CC BY license (http://creativecommons.org/licenses/BY/4.0/).

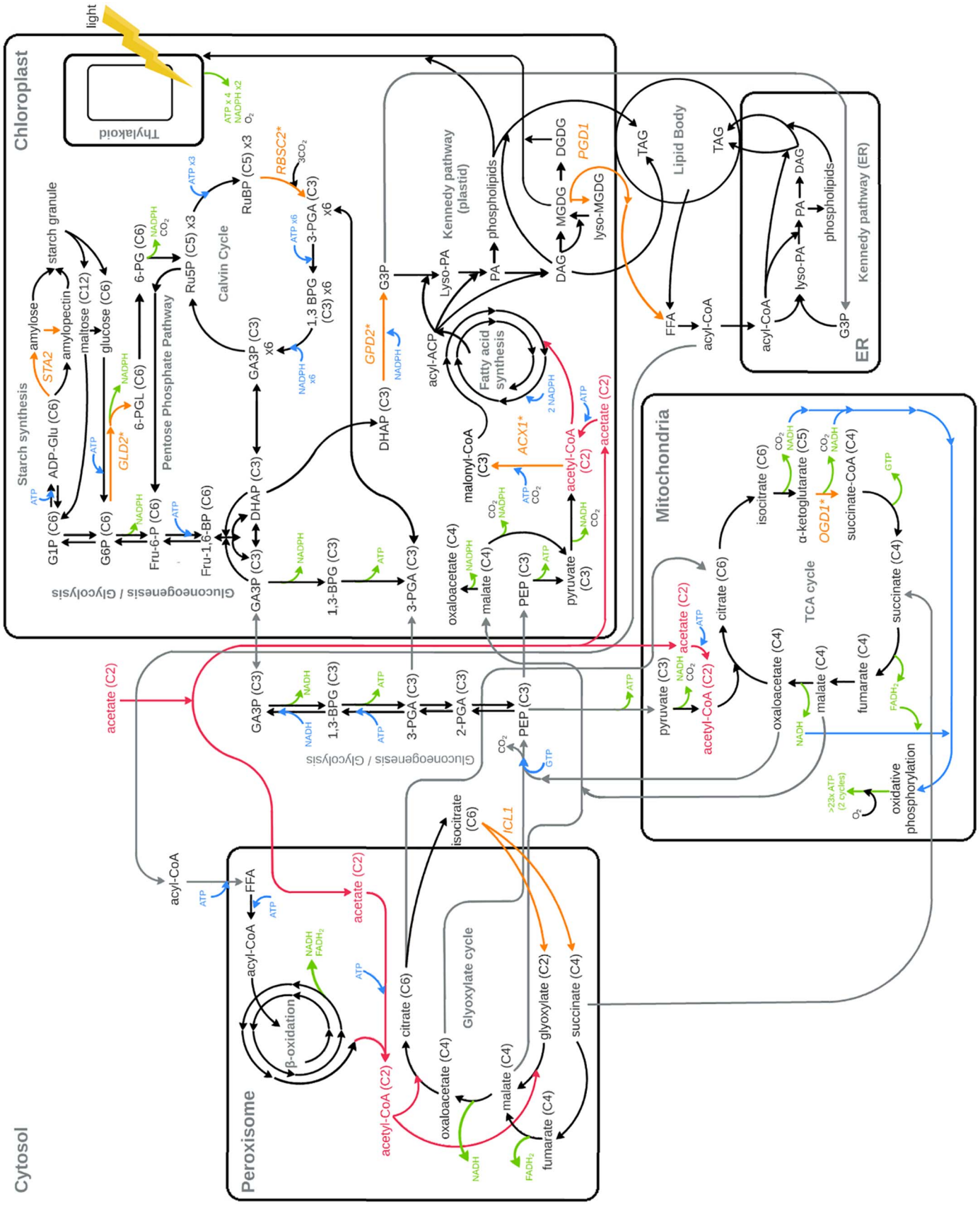
Cytosol
Chloroplast
Thylakoid
light
ATP x 4
NADPH x2
O2
Starch synthesis
starch granule
amylose
amylopectin
maltose (C12)
glucose (C6)
STA2
ADP-Glu (C6)
G1P (C6)
G6P (C6)
Fru-6-P (C6)
Fru-1,6-BP (C6)
GLD2*
6-PGL (C6)
6-PG (C6)
Pentose Phosphate Pathway
Ru5P (C5) x3
RuBP (C5) x3
Calvin Cycle
RBSC2*
3-PGA (C3) x6
1,3 BPG (C3) x6
GA3P (C3) x6
DHAP (C3)
GA3P (C3)
1,3-BPG (C3)
3-PGA (C3)
Gluconeogenesis / Glycolysis
GPD2*
G3P
Kennedy pathway (plastid)
Lyso-PA
PA
phospholipids
acyl-ACP
Fatty acid synthesis
malonyl-CoA (C3)
ACX1*
acetyl-CoA (C2)
acetate (C2)
oxaloacetate (C4)
malate (C4)
PEP (C3)
pyruvate (C3)
DAG
MGDG
DGDG
PGD1
lyso-MGDG
TAG
Lipid Body
FFA
acyl-CoA
ER
Kennedy pathway (ER)
Mitochondria
citrate (C6)
isocitrate (C6)
α-ketoglutarate (C5)
OGD1*
succinate-CoA (C4)
succinate (C4)
fumarate (C4)
TCA cycle
oxidative phosphorylation
>23x ATP (2 cycles)
Peroxisome
β-oxidation
Glyoxylate cycle
glyoxylate (C2)
ICL1

Fig. 1. Simplified diagram of the central carbon metabolism in *Chlamydomonas reinhardtii*. Pathways with redox cofactor inputs (ATP, NADH, and NADPH) are highlighted with a blue arrow, while outputs are highlighted with green arrows. Pathways for exogenous acetate derived acetyl-CoA metabolism are highlighted in red. Inter-organelle flux of metabolites is highlighted in grey. The targeted genes and the reactions associated with the enzymes they encode are highlighted in orange. The asterisk (*) symbol indicates that that gene of interest is one of multiple variants of the gene or encode one subunit of the enzyme involved in the reaction. FA import into the peroxisome is based on the *Arabidopsis* metabolism but may include import of FFA as in yeast [27]. Acetate is thought to be transported in to the cell via a monocarboxylate transporter [12]. Acetyl-CoA synthesis is thought to occur in multiple organelles via two alternative pathways as outlined in the text below. Gene abbreviations are: *ACX1*, α-carboxyltransferase subunit of plastidic multimeric acetyl-coA carboxylase; *GLD2*, glucose-6-phosphate dehydrogenase 2; *GDP2*, glycerol-3-phosphate dehydrogenase 2; *ICL1*, isocitrate lyase 1; *OCD1*, 2-oxoglutarate dehydrogenase, E1 subunit; *RBSC2*, ribulose-1,5-bisphosphate carboxylase/oxygenase small subunit 2; *PGD1*, plastid galactoglycerolipid degradation 1; *STA2*, starch synthase granule-bound 2. Metabolite abbreviations are: 1,3-BPG, 1,3-biphosphoglycerate; 2-PGA, 2-phosphoglycerate; 3-PGA, 3-phoshoglycerate; 6PG, 6-phospho-gluconate; 6-PGL, 6-phosphogluconolactone; ADP-Glu, ADP-glucose; ATP, adenosine triphosphate; DAG, diacylglycerol; DGDG, digalactosyldiacylglycerol; DHAP, dihydroxyacetone phosphate; FADH2, flavin adenine dinucleotide quinone; Fru-1,6-BP, fructose-1,6-bisphosphate; Fru-6-P, fructose-6-phosphate; G1P, glucose-1-phosphate; G3P, glycerol-3-phosphate; G6P, glucose-6-phosphate; GA3P, glyceraldehyde-3-phosphate; GTP, guanosine triphosphate; Lyso-PA, lyso-phosphatic acid; MGDG, monogalactosyldiacylglycerol; NADH nicotinamide adenine dinucleotide; NADPH, nicotinamide adenine dinucleotide phosphate; PA, phosphatic acid; PEP, phosphoenolpyruvate; Ru5P, ribose-5-phosphate. RuBP, ribulose-1,5-bisphosphate; TAG, triacylglycerol. Pathways based on references [18,27–36]. (For interpretation of the references to colour in this figure legend, the reader is referred to the web version of this article.)

step reaction involving acetate kinase (AK) and phosphate acetyltransferase (PAT). *C. reinhardtii* contains multiple copies of these genes with different putative localisations. Consequently it is assumed that acetyl-CoA is synthesised from acetate in multiple organelles [18] (Fig. 1).

Previous studies have demonstrated that increasing the concentration of exogenous acetate leads to a proportionate increase in TAG (up to 50 mM acetate) [19,20]. In contrast, starch accumulation does not follow this trend, becoming saturated at a lower acetate concentration. This indicates surplus carbon is directed to TAG accumulation once the capacity of starch storage is met [19]. This observation is supported by significantly elevated rates of TAG accumulation in a starchless mutant of *C. reinhardtii* when grown under N stress [12,21–23]. Another important component of TAG accumulation in *C. reinhardtii* is the requirement of light for high lipid accumulation, Fan et al. [19] reported that cultures grown under heterotrophic conditions accumulated negligible levels of TAG after 2 days of N deprivation.

Despite the advantages in productivity provided by mixotrophic growth, large scale microalgae cultivation for production of sustainable biofuels and bioproducts is typically envisaged to be carried out under autotrophic conditions using natural sunlight [24–26]. Given the apparent importance of both carbon availability and light for lipid accumulation, it is important to establish how the metabolic response to nitrogen deprivation under autotrophic conditions and a diurnal light cycle differs from the idealised conditions used in previous studies. Therefore, the research presented here was undertaken to elucidate the metabolic response of *C. reinhardtii* to N deprivation under autotrophic conditions and a diurnal light period. In order to maximise the scope of experimental treatments, a targeted high temporal resolution approach was taken utilising quantitative-reverse transcription PCR (q-RTPCR) coupled with physiological assays.

This study focused on 8 key genes involved in carbon input into TAG synthesis and the surrounding carbon metabolism which have been highlighted by previous transcriptomic studies as being particularly responsive to N deprivation and lipid accumulation (Fig. 1) [1,10,12]. Briefly, the genes include *RBSC2*, *OGD1*, *ICL1*, which encode for critical enzymes involved in the Calvin cycle, tricarboxylic acid (TCA) cycle and glyoxylate cycles respectively, representing the main routes of carbon input into the cell (see Fig. 1 for details). Analysis of expression of the gene *GLD2* was also undertaken, to monitor activity of the main alternative route of NADPH production (primarily produced via photosynthesis) via the pentose phosphate pathway, required for TAG and starch synthesis (Fig. 1). Expression of *ACX1* and *GPD2* was analysed, encoding enzymes involved in the initial fatty acid synthesis step and glycerol-3-phosphase (TAG backbone) synthesis. Due to the multiple genes involved in TAG synthesis, this work focused on genes involved in committal carbon inputs into FA synthesis rather than multiple fluxes to TAG involving acyltransferases. An exception, *PGD1*, a galactolipid lipase, was analysed in addition to monitor degradation from monogalactosyldiacylglycerol (MGDG), hypothesised to be differentially effected by both diurnal light regimes and organic carbon availability (Fig. 1). Finally, the gene *STA2*, encoding a key enzyme involved in starch synthesis was also analysed to elucidate activity of carbon flux into starch (Fig. 1). The role and justification for choosing these genes are detailed further in the Results section.

2. Materials and methods

2.1. Organism and growth conditions

The transcriptomic and physiological response of *C. reinhardtii* to N deprivation is strain specific and influenced by culture conditions [1,10,12]. Consequently, to facilitate cross-literature comparison, the experimental design of this study closely matched that used in the recently published mixotrophic transcriptomic experiment reported by Goodenough et al. [12].

Chlamydomonas reinhardtii cc-4349 (cw-15, mt$^-$) was obtained from the Chlamydomonas Resource Centre (University of Minnesota, USA). Previous transcriptomic research has been undertaken with the cc-4349 aiding comparison of data [1,10,12]. *C. reinhardtii* cc-4349 was maintained on an antibiotic HSMA agar plate as described in Kan and Pan [37].

Chlamydomonas reinhardtii cc-4349 was grown in HSM medium [38]. For mixotrophic growth treatments, the base medium was modified with the addition of 20 mM potassium acetate. Cultures were inoculated to an initial cell density of approximately 1.89×10^5 cells ml^{-1} and grown in 1000 ml Erlenmeyer flasks containing 500 ml of medium. Cultures were grown under 100 ± 5 μmols photon m^{-2} s^{-1} illumination and shaken continuously at 125 rpm at 25 °C ± 1. This light intensity is higher than the conditions used in Goodenough et al. [12], but was necessary to maintain reasonable autotrophic growth rates. Cultures were grown under either a 12-hour light, 12-hour dark photoperiod (12*L*) or a 24-hour light continuous photoperiod (24 L). In total, five treatments were cultivated as shown in (Table 1).

An outline of the experiment design is provided in Fig. 2. For nitrogen starvation experiments, cultures were grown to approximately 4×10^6 cells ml^{-1} at exponential phase before harvesting by centrifugation (1250 *g* for 3 min at 15 °C). Cells were resuspended in 500 ml of fresh HSM or HSMA media lacking NH_4Cl (nitrogen free, NF). Transfer to nitrogen free media was carried out without a washing step to avoid cell loss (as in [12]). The control treatment was resuspended in nitrogen replete medium. Cultures treated with a 12 L photoperiod were synchronized with several light/dark cycles before harvesting.

Table 1
Treatment conditions.

Treatment	Acetate	Light period (hours)	Nitrogen
M-24-C	+	24	+
M-24-NF	+	24	−
M-12-NF	+	12	−
A-24-NF	−	24	−
A-12-NF	−	12	−

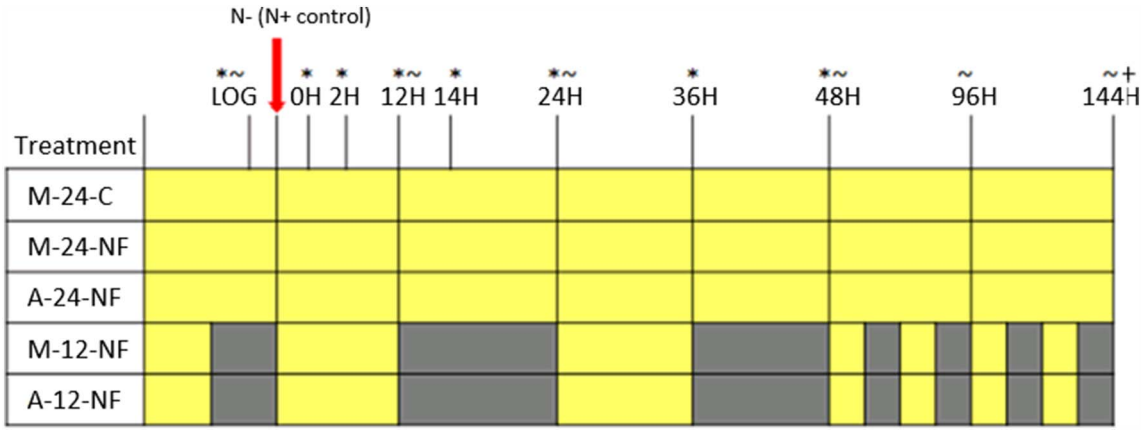

Fig. 2. Experimental scheme for sampling. H indicates number of hours from point of resuspension. LOG, indicates sampling point at which cells were in the log (exponential) phase of growth, immediately before transfer to N deplete (−N) medium. The symbol * indicates RNA sampling time points (sample was not taken at 36H for 24 L treatments). The symbol ~ indicates biochemical sampling (including chlorophyll, TAG, starch, and acetate assays). The symbol + indicates sampling for FAME quantification and fluorescence microscopy. Yellow boxes indicate time periods of illumination. Grey boxes indicate dark periods. Red arrow indicates beginning of the experiment with all cells resuspended in the appropriate medium/conditions. For definitions of treatment names see Table 1. (For interpretation of the references to colour in this figure legend, the reader is referred to the web version of this article.)

Resuspension took place at the end of the dark period, placing cultures back into illumination for 12 h after resuspension (Fig. 2).

For RNA expression analysis, a sample was taken immediately before resuspension into NF media (LOG), immediately after resuspension (0 h), followed by sampling at 2, 12, 14, 24 and 48 h. For 12 L and control cultures, an additional sample was taken at 36 h in order to sample 2 points (12 and 36 h) after 12 h illumination (Fig. 2). Sampling immediately after resuspension was intended to allow distinction of RNA change associated with cell handling rather than nitrogen stress [11]. Biochemical analyses were taken at LOG, and 12, 24, 48, 96 and 144 h after resuspension in NF media. Cell counts were taken with every sampling point. Treatments were carried out in triplicate.

2.2. Triglyceride assay

A novel enzymatic method for TAG quantification was developed in the Goodenough lab, University of Washington (Weiss and Goodenough, personal communication) and adapted for this investigation. The protocol utilises a commercial enzymatic triglyceride reagent (Infinity Triglyceride Regent, ThermoScientific). The reagent contains a TAG lipase (9001-61-1) which lyses TAG and releases a glycerol molecule. The free glycerol then goes through a series of reactions to produce a red coloured quinoneimine dye proportional to the initial TAG concentration. The lipase used in this analysis preferentially targets TAG molecules, then DAG and MAGs, leading to the release of glycerol [39]. Consequently, glycerolipid precursors DAG and MAG will also be quantified. However, these precursor lipids are negligible compared to TAG concentration, particularly when under N stress [30]. Glycerol is used as a standard for this quantification because oil standards cannot be solubilised effectively in the reagent, and therefore will not be efficiently broken down by the lipase (Weiss, personal communication 2015).

In this protocol, a 4 ml aliquot of culture of known cell density was centrifuged at 2500 *g* for 5 min. The pellet was resuspended in 0.4 ml of dH_20 and frozen at −20 °C for storage. For processing, the sample was defrosted and lysed using a bead mill homogeniser (1 min at 2700 rpm). The sample was checked microscopically to ensure ~100% of the cells were lysed. Samples were kept on ice before and after the lysing procedure.

In order to measure background free glycerol a blank cold run was carried out to inhibit lipase activity (but not downstream reactions). For the sample blank, working quickly, a 20 µl sample of lysed cells was added to 380 µl of cold (4 °C) triglyceride regent on ice. For the standard blank the lysed cells were replaced with 20 µl dH_20. The tubes were inverted slowly 10 times to mix, then centrifuged at 16000 *g* for 1 min at 4 °C. Avoiding the pellet, 300 µl of sample supernatant was immediately transferred to a plastic cuvette with 700 µl cold (4 °C) dH_2O. The cuvettes were wiped to remove condensation and the absorbance at 520 nm was recorded.

For the lipase active hot run the procedure is repeated at an elevated temperature. The sample reaction was prepared with 20 µl lysed cells and 380 µl reagent (at room temperature). The standard reaction was prepared by the addition of 4 µl of glycerol (2.82 mM, 2.5 mg ml^{-1} triolein equivalent), 16 µl dH_20, and 380 µl reagent. After mixing, the samples were incubated at 37 °C for 10 min then spun down. Following centrifugation, the samples were diluted and absorbance was measured as detailed above. TAG concentration was calculated relative to the glycerol standard (Supplementary Material 1).

2.3. Fatty acid profile and quantification

For FAME analysis a 100 ml aliquot sample was taken from each culture at the end of the nitrogen deprivation experiment (144 h, Fig. 2). The sample was washed and lyophilised. Samples were then processed using an in-situ direct transesterification method adapted from [40,41], using tridecanoic acid and pentadecane as internal standards.

Samples were analysed by gas chromatography mass spectrometry (GC–MS) using an AutoSystem XL Gas Chromatograph (CHM-100-790, Perkin Elmer) coupled with a TurboMass Mass Spectrometer (13657, Perkin Elmer). The GC was fitted with a Zebron™ ZB-5 ms, 30 m × 0.25 mm ID × 0.25 µm FT (7HG-G010-11, Phenomenex) GC capillary column. Samples were injected (5 µl volume) via an autosampler onto the column and eluted at an injection temperature of 250 °C with a 100:1 split ratio and a He constant carrier flow (1 ml min^{-1}). The temperature programme was set to 120 °C, held for 1 min, 140 °C at 5 °C min^{-1}, held for 2 min 170 °C at 2 °C min^{-1}, held for 2 min, and finally 250 °C at 1 °C min^{-1}. The mass spectrometer was operated in electron ionisation (EI+) mode. Start mass was set to 50 and end mass to 600. Scan time was 90 min. Turbomass software (Ver 5.2.4) was used to quantify each FAME using a predetermined response factor [40].

2.4. Fluorescence microscopy

For qualitative analysis of neutral lipid accumulation, Nile red fluorescence microscopy was carried on samples taken after 144 h of N stress using the method outlined in [42]. Ten ml aliquots of each sample

were spun down and resuspended in 1 ml of 2% DMSO with 2 mg/l Nile red and left to incubate for 10 min. Fluorescence was observed using a fluorescence microscope (Eclipse E400, Nikon), with an excitation wavelength of 450–490 nm. Images were processed with LUCIA G (Ver 3.1) software.

2.5. Starch assay

Starch content was determined using a commercial amyloglucosidase/α-amylase enzymatic starch kit (K-TSTA, Megazyme). In this protocol a 4 ml aliquot of culture, of known cell density, was lyophilised and processed following the method outlined in Laurens et al. [43,44].

2.6. Acetate assay

Supernatant acetate concentration was determined using a commercial acetic acid assay kit (K-ACETRM 07/12, Megazyme). In this method, a 200 µl aliquot of supernatant was diluted with 800 µl dH_20. The sample was processed according to manufacturer's instructions, using a 96 well microplate and microplate reader, fitted with 340 nm absorbance filter. Each biological replicate was measured with 4 technical repeats.

2.7. Chlorophyll assay

Chlorophyll assays were conducted using a 3 ml aliquot of culture. Cells were lysed with a bead mill homogeniser and extracted using a 90% acetone mixture and quantified by absorbance at 647 and 664 nm as described in [45].

2.8. Maximum quantum efficiency of PSII (F_v/F_m)

Cell samples were concentrated to a density of 5.67×10^7 cells ml^{-1}, 2 ml aliquots of the cell concentrate were added to a 6 multiwell plate (2 technical and 3 biological replicates) and dark adapted for 30 min [46]. Minimal (F_o) and maximal fluorescence (F_m) before and after a saturating light pulse was measured using a Maxi IMAGING-PAM chlorophyll fluorimeter, fitted with an IMAG-MAX/LR measuring head (Heinz Waltz GmBh), and recorded using ImagingWinGigE software (V2.45i). The F_o and F_m were used to calculate F_v/F_m. The equipment settings used for analysis were; Special Saturation Pulse (SP) routine settings, ML 3, Gain 20, Frequency 2, Damping 2. In this protocol, a parallel series of cultures were grown using the treatments and growth conditions described in Fig. 2. Samples were taken immediately before resuspension (LOG), followed by 24, 48, 96 and 144 h after resuspension.

2.9. RNA extraction

The method of RNA extraction was adapted from [12] using a commercial RNA extraction kit (Purlink™ RNA Mini, Ambion®, Life Technologies) coupled with TRIzol® reagent (Ambion®, Life Technologies). In this protocol, a 10 ml aliquot of culture was transferred, at the time points indicated in Fig. 2, and centrifuged at 2500 *g* for 5 min at 15 °C. The supernatant was immediately removed and the pellets were snap frozen in liquid N_2 and stored at −80 °C.

For RNA extraction, an 0.8 ml aliquot of TRIzol® reagent was added to each sample. Samples were homogenised by gentle pipette trituration and left to incubate for 5 min at room temperature to allow for complete dissociation of nucleoprotein complexes. The TRIzol® mixture was centrifuged at 600 *g* for 2 min at 15 °C to remove starch. Following centrifugation, phase separation and purification was carried out using the TRIzol® Plus RNA purification kit, following the manufacturer's protocol. An on-column Purlink DNase solution was used to remove contaminating gDNA. RNA concentration and purity was assessed using a nanospectrophotometer (Jenway Genova Nano, Bibby Scientific). RNA quality was assessed via a 0.8% ethidium bromide stained agarose gel. Two clear 28S and 18S RNA bands indicated low RNA degradation. The 18S band was occasionally seen as a triplet due to the smaller prokaryotic (16S) chloroplast and mitochondrial RNA.

2.10. Quantitative reverse transcription PCR (qRT-PCR)

Complementary (c)DNA synthesis and amplification was carried out using a one-step Brilliant III Ultra-Fast SYBR® Green QRT-PCR Master Mix kit (Agilent), using a primer concentration of 0.3 µM. qRT-PCR was performed using a Mx3005P instrument (Agilent) following hot start fast reaction conditions. A disassociation curve analysis was performed after amplification cycling to assess the presence of a single amplicon product. With each run and primer pair, a no-template control and no-reverse transcriptase control were also analysed.

Primers for 8 genes of interest and 5 reference genes were designed through a series of steps following MIQE guidelines for qRT-PCR experiments [47,48]. Primer pairs were designed using a combination of the online software QuantPrime [49] and the standalone software Beacon Designer™ (Ver. 8.10, Premier Biosoft). Primers and amplicon products were assessed for secondary structures using Beacon Designer Free Edition (http://www.premierbiosoft.com), and IDT Unafold (https://www.idtdna.com/UNAFold). The efficiency of each primer was analysed by a two-step protocol as recommended by [50], first using an eleven point dilution standard curve to determine a log-linear RNA concentration range, followed by a 5 point serial dilution within the log linear range to calculate the efficiency of the primer. The primer pairs used and efficiency are shown in Supplementary material 2.

The four reference genes targeted for initial stability assessment were; ubiquitin-like protein (*UBQ2*, Cre09.g396400), receptor of activated protein kinase C (*RCK1*, Cre06.g278222, previously annotated as, *CBLP*, Cre13.g599400), eukaryotic translation initiation factor (*EIF1A*, Cre02.g103550) and calvin cycle protein (*CP12*, Cre08.g380250). The stability of the selected reference genes was assessed by comparing gene expression across the range of treatments using the NormFinder Excel Add-in (Ver. 2, Department of Molecular Medicine, Aarhus University Hospital) to rank the expression stability of the reference genes under different treatment conditions [51]. The tool ranked *CP12*, *EIF1A* and *RCK1* to be the best combination of reference genes for stability. Subsequent experiments used these genes for normalisation.

Due to the large number of samples, each transcript analysed was spread over 7 plates and therefore were vulnerable to significant run-to-run variation [52]. To correct for this variation 6 inter-run calibrators (IRC, 3 biological, 2 technical) were analysed with each plate. The IRCs were identical samples with the same RNA samples and primers pairs which were added to every plate run [52]. The qBase qRT-PCR model (Biogazelle) was adapted to convert Cq values into normalised linear relative quantities, allowing normalisation with multiple reference genes and IRCs. Furthermore, as suggested by Hellemans et al. [52] expression data is presented as a fold change relative to arithmetic average of all Cq values across all samples for that transcript. The model and minor alterations are outlined in Supplementary material 3.

2.11. Statistics

All results are presented as mean values. The effect of growth conditions on measured observations (inter-treatment variation) were statistically analysed using a two-sample *t*-test, assuming unequal variance. The statistical significance of differences between measurements taken at different time points within the same treatment (intra-treatment variation) was analysed using a paired two sample t-test. All analyses were carried out with the statistical software R (v.3.1.2, R).

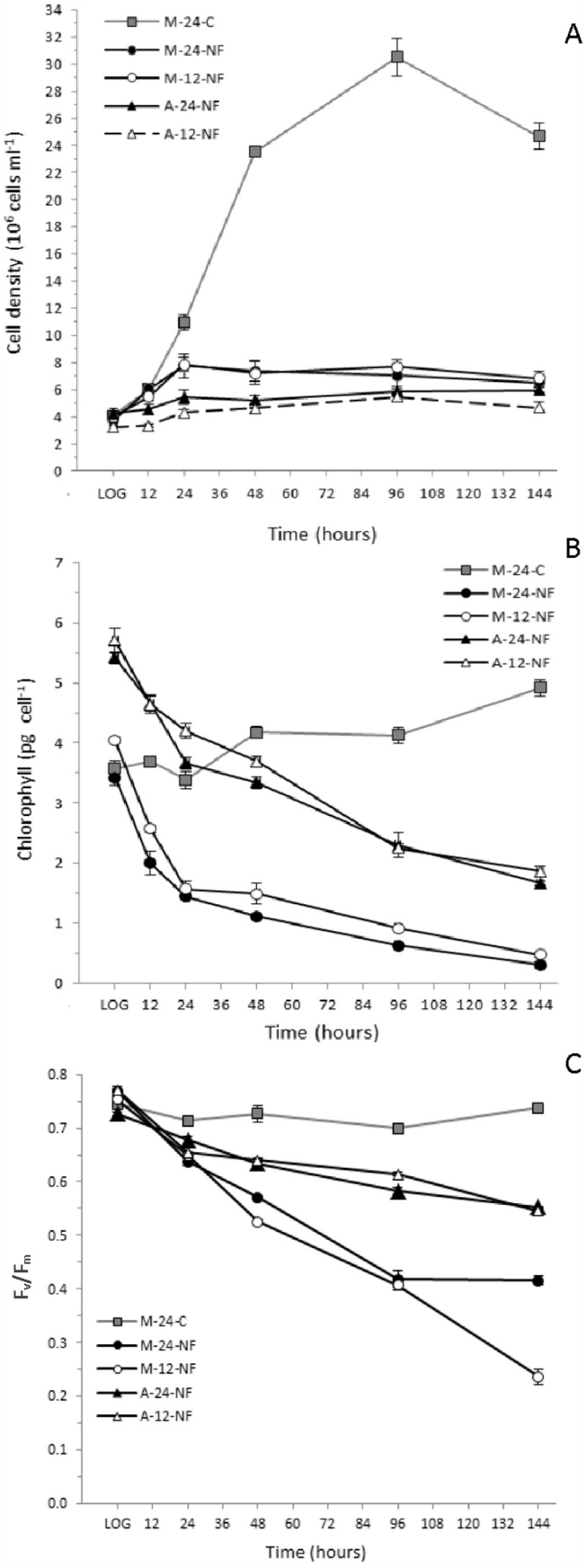

Fig. 3. A). Growth curve of *C. reinhardtii* after cell resuspension into nitrogen free (NF) or replete (C) medium. **B)** Chlorophyll concentration (pg cell^{-1}) before (LOG) and after cell resuspension in nitrogen free (NF) or replete (C). **C)** Maximum quantum yield of PSII (F_v/F_m) before (LOG) and after cell resuspension in nitrogen free (NF) or replete (C) medium. LOG, indicates sampling point at which cells were in the log (exponential) phase of growth, immediately before transfer to N deplete (−N) medium. Treatment conditions are outlined in Table 1, M-24-C, mixotrophic continuous light, C medium; M-24-NF, mixotrophic continuous light NF medium; M-12-NF, mixotrophic diurnal light, NF medium; A-24-NF, autotrophic continuous light, NF medium; A-12-NF, autotrophic diurnal light, NF medium. Error bars represent SE ($n = 3$).

3. Results

3.1. Cell growth and photosynthetic degradation

Upon nitrogen deprivation, cells in all treatments continued to divide for 24 h before the cessation of growth (Fig. 3a), but at the expense of chlorophyll content (Fig. 3b). Cell density in both mixotrophic treatments doubled (2.1 fold increase for M-24-NF, 2.0 fold increase for M-12-NF), while chlorophyll content dropped by 58–61% ($p < 0.01$). Consequently, this drop indicates inhibition of chlorophyll synthesis as cell divide (leading to chlorophyll content splitting between cells). Unlike the trend reported in [1], chlorophyll content continued to fall beyond the cessation of cell growth (post-24 h), indicating degradation of existing chlorophyll. On the sixth day of N deprivation chlorophyll content had been reduced by 91% and 88% for M-24-NF and M-12-NF respectively ($p < 0.001$); the effect of the daily dark period on this degradation appears to be negligible for mixotrophic cultures ($p > 0.05$). As expected, the cell growth of autotrophic treatments was comparatively modest, increasing by approximately 30% in both A-24-NF and A-12-NF (29% and 33%, respectively) in 24 h. This growth was mirrored by a drop in chlorophyll content by 32% and 26% (not significantly different, $p > 0.05$), beyond this point chlorophyll was degraded further reaching a 69% and 67% reduction by 6 days for A-24-NF and A-12-NF respectively, with no significant difference ($p > 0.05$) between autotrophic treatments. Interestingly, beyond the initial growth period (post-24 h NF), autotrophic treatments had a 2-fold higher rate of chlorophyll degradation (pg cell^{-1} d^{-1}) compared to mixotrophic treatments, but retained more chlorophyll content after 6 days due to higher initial concentrations. Conversely, control cultures grown under N replete mixotrophic conditions continued log growth, reaching stationary phase between 48 and 96 h, beyond which the chlorophyll content increased significantly ($p < 0.05$) by 37%, perhaps due to the exhaustion of acetate and a shift towards autotrophy [53].

In order to determine the integrity of photosynthetic machinery (particularly PSII) the maximum quantum efficiency of PSII (F_v/F_m) was tracked before and after cell resuspension in N deplete conditions (Fig. 3c). In support of the trend of chlorosis, F_v/F_m measurements indicated a more rapid decline of photosynthetic capacity in mixotrophic treatments compared to autotrophic treatments, while the maximum quantum efficiency of the control treatment did not significantly alter over the 144 h time period ($p > 0.05$). Again, the effect of photoperiod was minor until the last 48 h, when the F_v/F_m of M-12-NF continued to decline, while M-24-NF stabilised. The final fold reduction in mean F_v/F_m ratio was 1.8 fold in M-24-NF, 3.2 fold in M-12-NF, 1.3 fold in A-24-NF and 1.4 in A-12-NF over 144 h.

3.2. Central carbon metabolism

Significant degradation of photosynthetic apparatus has been shown to be concurrent with a shift in the central carbon metabolism towards dominance of catabolic fuelled respiratory energy generation [1]. The degree of photosynthetic degradation and availability of light may alter this shift and impact on the accumulation of carbon storage molecules.

QRT-PCR was performed to quantify gene expression throughout the experiment. The results are presented as fold change in expression

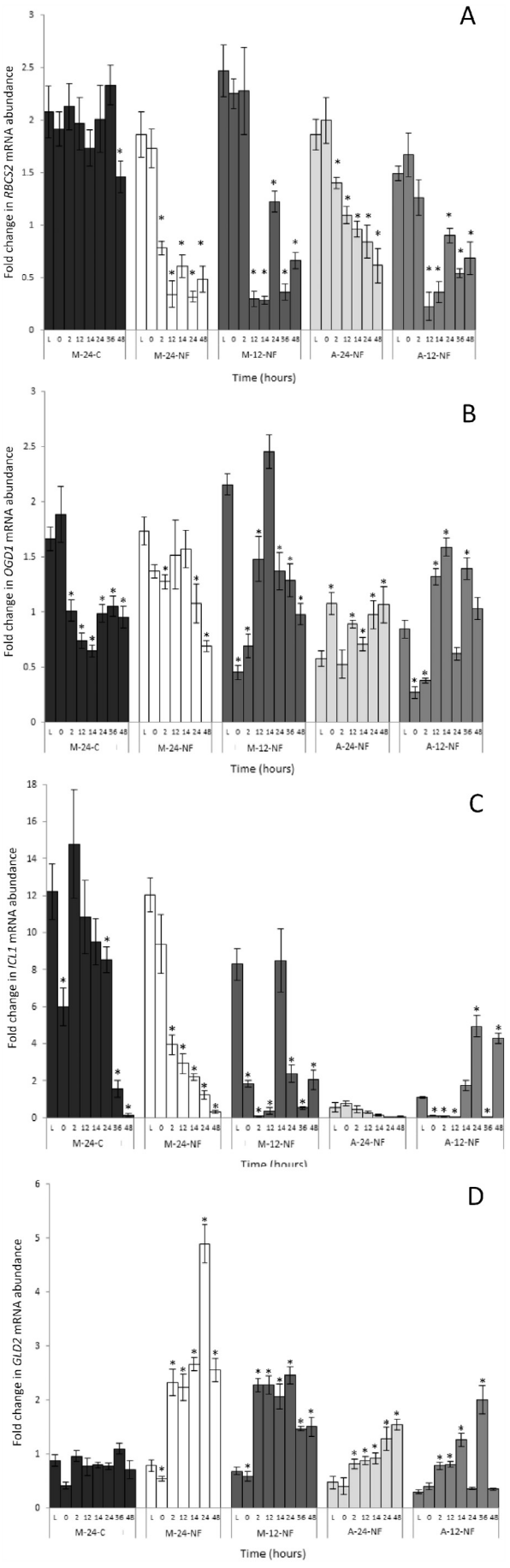

Fig. 4. Fold change (relative to the average expression of gene across all samples, time points and treatments) of, **A)** *RBSC2* **B)** *OGD1* **C)** *ICL1* **D)** *GLD2* gene expression, before (L) and after resuspension in nitrogen free (NF) or replete (C) medium. Referencing genes used for normalisation in this and all subsequent qRT-PCR were *GAPHD, EIF1A and RCK1*. LOG, indicates sampling point at which cells were in the log (exponential) phase of growth, immediately before transfer to N deplete (−N) medium. Treatment conditions are outlined in Table 1, M-24-C, mixotrophic continuous light, C medium; M-24-NF, mixotrophic continuous light, NF medium; M-12-NF, mixotrophic diurnal light, NF medium; A-24-NF, autotrophic continuous light, NF medium; A-12-NF, autotrophic diurnal light, NF medium. Error bars represent SE ($n = 3$).

relative to the average expression of that gene across all treatments and time points [52]. The degradation of photosynthetic machinery, highlighted in the previous section, was mirrored by a significant ($p < 0.01$) downregulation of the *RBSC2* gene (Cre03.g120150) in all N deprived treatments (Fig. 4A). The gene *RBSC2* encodes for the small subunit 2 of ribulose 1,5-bisphosphate carboxylase/oxygenase (RuBisCO), a highly abundant enzyme responsible for the carboxylation of ribulose-1,5-bisphosphate (RuBP), the first major step of CO_2 sequestration within the Calvin cycle (Fig. 1). Downregulation of *RBSC2* is correlated with an increase in RuBP and other Calvin cycle metabolites, indicating a reduced Calvin cycle flux [1]. Differences in the downregulation of *RBSC2* between treatments may give an insight into different responses to N stress. As expected, the degree and rate of *RBSC2* downregulation was significantly increased under mixotrophic conditions; after 12 h in N free medium *RBSC2* transcript abundance dropped 5 fold in M-24-NF between 0 and 12 h, compared to a 1.7 fold drop in A-24-NF. Cultures grown under a light/dark cycle had a similar fold reduction over the 48-h period measured compared to respective continuous light cultures, however, the downregulation was delayed until 12 h post deprivation (7.5 fold and 4.5 fold drop between 2 and 12 h, $p < 0.05$). Expression of *RBSC2* remained depressed until the beginning of the second light period at 24 h, when transcript abundance significantly increased ($p < 0.05$) in both 12 L treatments. This subsequent increase, and repeated fluctuations at 36 and 48 h, indicates that the well reported circadian rhythm of *RBSC2* expression [54,55] continues under N stress conditions. In comparison, *RBSC2* expression in the control treatment remained relatively stable with the exception of a comparatively moderate (37%) but statistically significant ($p < 0.05$) decline in expression between 24 and 48 h.

Expression of *OGD1* (Cre12.g537200) was measured to determine regulation of the tricarboxylic acid (TCA) cycle and cellular respiration after N deprivation. The *OGD1* gene encodes the 2-oxoglutarate dehydrogenase E1 subunit of the α-ketoglutarate dehydrogenase enzyme complex, a key catalyst in the TCA cycle involved in the decarboxylation of α-ketoglutarate releasing reductive NADH which goes on to drive mitochondrial oxidative phosphorylation (ATP synthesis, Fig. 1). In agreement with previous studies [10,12], *OGD1* expression in M-24-NF, declined slowly between LOG and 48-h NF (2.5 fold decline, $p < 0.001$, Fig. 4B). In contrast A-24-NF cultures experienced a moderate but significant increase in *OGD1* expression over the experiment (1.85 fold, $p < 0,05$), but from a significantly lower initial transcript abundance (3 fold lower, $p < 0.01$) compared to M-24-NF. Expression of *OGD1* in the nitrogen replete control culture, M-24-C, also dropped (1.6 fold, $p < 0.01$) over the first 2 h but then remained relatively stable.

As expected, the diurnal trend observed in *OGD1* expression was inverse to the pattern measured in *RBSC2*, with expression dropping immediately after resuspension (and illumination) between LOG-0 h in both M-12-NF (4.7 fold drop, $p < 0.01$) and A-12-NF (3 fold drop, $p < 0.05$). Expression was then upregulated immediately before (12h) and after (14 h) darkness: 3.45 fold and 4.3 fold ($p < 0.001$) increase in M-12-NF and A-12-NF respectively between 2 and 14 h. The trend was repeated again between 24 and 48 h in A-12-NF, but not M-12-NF.

The *ICL1* gene (Cre06.g282800) encodes for isocitrate lyase, a key enzyme specific to the glyoxylate cycle (Fig. 1). The sequential action of

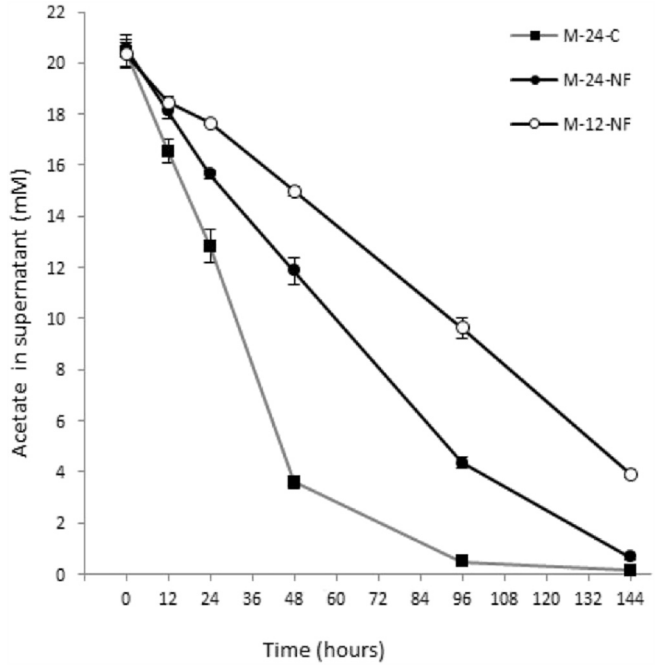

Fig. 5. Concentration of acetate in supernatant (mM) of mixotrophic treatments. Treatment conditions are outlined in Table 1, M-24-C, mixotrophic continuous light, C medium; M-24-NF, mixotrophic continuous light, NF medium; M-12-NF, mixotrophic diurnal light, NF medium. Error bars represent SE (n = 3).

isocitrate lyase (cytosolic) and malate synthase (peroxisomal) is critical to the formation of C4 acids from 2 acetyl-CoA units (C2), bypassing two oxidative and CO_2 evolving steps in the TCA cycle, and thus enabling growth on C2 compounds [32,36]. These C4 molecules can then be fed into the gluconeogenesis and other biosynthesis pathways or be used to replenish intermediates in the TCA cycle [32,56]. This peroxisome/cytosol localised pathway has recently been demonstrated to play a predominant role in the assimilation of acetyl-CoA derived from acetate and fatty acids (via peroxisome localised β-oxidation FA degradation) in *C. reinhardtii* [32,34,36]. Consequently, *ICL1* expression provides an indication of the assimilation pathway of acetate and activity of FA degradation. In the control treatment, M-24-C, following an initial dip immediately after resuspension, *ICL1* expression remains relatively steady (although with large variance, Fig. 4C). After 36 h there is a significant downregulation of *ICL1* which correlates with rapid exhaustion of acetate (Fig. 4C). In contrast, *ICL1* expression in M-24-NF is suppressed after 2 h (3-fold decline, LOG-2 h, $p < 0.05$) and continued to decline reaching a 33.4 fold drop by 48 h (LOG-48 h, $p < 0.001$), despite high acetate availability and continued acetate consumption (Fig. 4C and 5). Unsurprisingly, A-24-NF treatments, with no acetate supplementation, had very low initial expression rates, which did not significantly alter throughout the experiment ($p > 0.05$).

Unlike M-24-NF, *ICL1* expression in M-12-NF dropped immediately after resuspension (0 h), and continued to reduce 110 fold over 2 h (LOG-2 h, $p < 0.001$). Furthermore, 2 h into the first NF dark period (14 h), *ICL1* expression ramped back up to pre-deprivation levels (115 fold increase, 2–14 h, $p < 0.001$), then dropped immediately before (24 h) and further after (36 h) the second period of illumination. This diurnal pattern was also evident in the A-12-NF treatment, despite no acetate supplementation. Transcript abundance increased 41 fold ($p < 0.05$) between 12 and 14 h, and continuing to increase to 24 h (113 fold increase 12–24 h, $p < 0.01$). Similarly, expression dropped sharply during the second period of illumination (218 fold reduction, 24–36 h, $p < 0.001$) and increased over the second dark period darkness (187 fold, 36–48 h, $p < 0.01$). Despite the higher *ICL1* expression at night, the rate of acetate consumption in M-12-NF dropped by 57% compared to consumption between 0 and 12 h (rate calculated as difference in acetate consumption between two time points divided by period of time), while M-24-NF consumption remained constant (Fig. 5). The overall rate of acetate uptake (between 0 and 48 h) was 350 μmols hr^{-1} for M-24-C, 181 μmols hr^{-1} for M-24-NF and 112 μmols hr^{-1} for M-12-NF, which is comparable to the rate observed in [12] (193 μmols hr^{-1} for similar cell density M-24-NF treatment).

The oxidative phase of the pentose-phosphate pathway (OPPP) acts as an alternative route to upper stage of glycolysis, oxidising glucose-6-phosphate to the intermediate ribose-5-phosphate, producing 2 NADPH molecules and 1 CO_2 (Fig. 1). NADPH is a reducing agent required for anabolic reactions, particularly fatty acid synthesis (14 NADPH per C16:0 FA, 62 NADPH per C16:0 FA if acetyl-CoA production included) [29]. The major alternative pathway for NADPH production is the last stage (PSI) of the photosynthetic linear electron transport, consequently a degradation of the photosynthetic machinery is likely to lead to a simultaneous upregulation of the OPPP pathway, particularly if NADPH demand is maintained through lipid synthesis. The *GLD2* gene (Cre08.g378150), encodes for the enzyme glucose-6-phosphate dehydrogenase (Fig. 1). This enzyme is involved in the first step in the PP pathway, the conversion of glucose-6-phosphate into 6-phosphogluconolactonase (producing 1 NADPH, Fig. 1). Goodenough et al. [12] demonstrated that nitrogen stress induced an upregulation of *GLD2* and downstream OPPP genes in mixotrophic *C. reinhardtii* under continuous light (similar to M-24-NF); however the impact of different light and carbon regimes on the activity of glucose-6-phosphate breakdown through the OPPP is not known. As expected, *GLD2* expression in M-24-NF was upregulated rapidly, increasing 3 fold after 2 h in NF medium (LOG-2 h, $p > 0.05$) (Fig. 4D). Expression remained stable, with the exception of a spike at 24 h (1.8 fold increase between 14 and 24 h, $p < 0.001$). The expression trend was very similar in M-12-NF, increasing 3.3 fold after 2 h (LOG-2 h, $p < 0.01$) and remaining stable, with the exception of a small drop (1.64 fold, $p < 0.05$) after 36 h. The gene *GLD2* was also upregulated in autotrophic treatments although at a more gradual rate, increasing 3.1 fold ($p < 0.01$) over 48 h for A-24-NF. However, the peak expression was 3.2 fold lower than M-24-NF. Expression of *GLD2* in A-12-NF increased at a similar rate to A-24-NF, however expression dropped at 24 h (3.5 fold drop, $p < 0.05$) and 48 h (5.9 fold drop, $p < 0.05$), and is assumed to be downregulated (or post 14 h) during the dark period.

3.3. Starch accumulation under nitrogen deprivation

Starch accumulation was assessed via an amyloglucosidase/α-amylase starch assay and by tracking the expression of *STA2* (Cre17.g721500). *STA2* has been highlighted as a key and highly responsive gene that encodes the granule-bound starch synthase (GBSS1) enzyme, involved in the biosynthesis of amylose (and structure of amylopectin) components of starch [57–59] (Fig. 1). N deprivation led to an increase in cellular starch concentration in all treatments between 0 and 6 days ($p > 0.001$); however, the degree and trend of accumulation and the expression of *STA2* were influenced by both photoperiod and organic carbon supplementation (Fig. 6A and B).

There was clearly a diurnal response to starch accumulation in both 12 L treatments. Expression of *STA2* was tightly correlated to photoperiod, decreasing immediately before and during the dark period, and increasing at the onset of the light period. Log-phase samples (taken at the end of the dark period) had higher *STA2* expression, particularly in M-12-NF cultures (25.4-fold higher expression than M-24-NF, $p < 0.001$). The starch concentration in 12 L treatments, at this first LOG phase time point, was significantly higher relative to corresponding continuous light treatments, 2.6 fold higher ($p < 0.001$) in M-12-NF and 4.3 fold higher ($p < 0.001$) in A-12-NF. After resuspension in NF media and exposure to light, *STA2* expression in both 12 L treatments was immediately upregulated (3.57 and 3.02 fold for M-12-

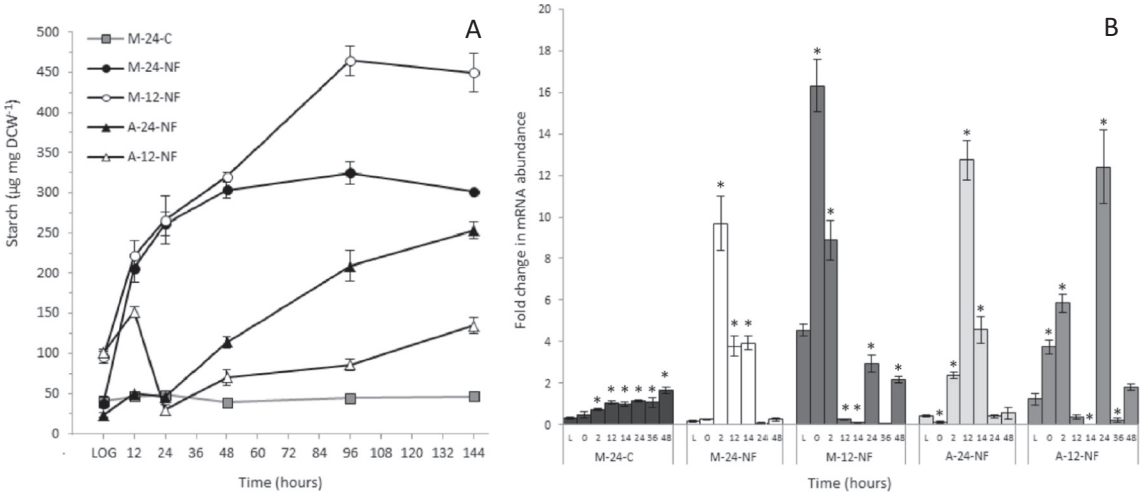

Fig. 6. A) Starch content (µg starch mg^{-1}DCW) before (LOG) and after cell resuspension in nitrogen free (NF) or replete (C) medium. **B)** Fold change (relative to the average gene expression of all samples across all time points and treatments) of *STA2* expression, before (L) and after resuspension in nitrogen free (NF) or replete (C) medium. LOG (L), indicates sampling point at which cells were in the log (exponential) phase of growth, immediately before transfer to N deplete (−N) medium. Treatment conditions are outlined in Table 1, M-24-C, mixotrophic continuous light, C medium; M-24-NF, mixotrophic continuous light, NF medium; M-12-NF, mixotrophic diurnal light, NF medium; A-24-NF, autotrophic continuous light, NF medium; A-12-NF, autotrophic diurnal light, NF medium. Error bars represent SE ($n = 3$), * symbols indicate significant difference from L (LOG) time point values (*t*-test, $p < 0.05$). For M-12-NF and A-12-NF, L sample taken in dark period before resuspension, then 0 to 12 h light; 12 to 24 h dark; 24 to 36 h light; 36 to 48 h dark.

NF and A-12-NF, respectively, $p > 0.01$). In contrast, the response of 24 L treatments was slower, with *STA2* expression increasing (and peaking in M-24-NF) after 2 h of N stress. At the 12-h time point, immediately before the onset of the dark period, *STA2* expression significantly decreased (34.7 and 16.3-fold reduction between 2 and 12 h for M-12-NF and A-12-NF respectively, $p < 0.001$). This diurnal trend repeated, with a substantial increase in *STA2* expression at 24 and 48 h, and a large drop at 36 h. Comparatively, in M-24-NF and A-24-NF cultures, *STA2* expression peaked within the first 12 h then subsequently declined linearly, a trend that was reported (for M-24-NF treatments) in Goodenough et al. [12].

Organic carbon supplementation also influenced starch accumulation and *STA2* expression trends. As may be expected, the rate of starch accumulation in mixotrophic treatments was significantly higher (7 fold and 2.5 fold for M-24-NF and M-12-NF relative to autotrophic equivalents, $p < 0.01$) in the first 12 h of N deprivation (Fig. 6A). This higher accumulation rate correlates to an earlier peak in *STA2* expression in mixotrophic cultures. Organic carbon availability also impacted levels of starch catabolism during dark periods in 12 L treatments. During the first dark period (12–24 h) starch in the A-12-NF cultures dropped to a concentration significantly below that of the initial log-phase concentration ($p < 0.01$). Although no further measurements were taken at 12 h periods (i.e. at the end of the light period), it is likely that this diurnal drop repeated, leading to a reduced final concentration compared to A-24-NF (134.3 vs 253.5 µg starch mg^{-1} DCW, Fig. 6A). In contrast, in mixotrophic cultures, although starch accumulation in M-12-NF did abate during the first dark period, the reduction was similar to the trend observed in the continuous light treatment, M-24-NF. Beyond the 48-h time point, unlike M-24-NF, M-12-NF cultures continued to accumulate starch for a further 48 h.

3.4. TAG accumulation under nitrogen deprivation

Accumulation of TAG was monitored using a commercial glycerol assay, and analysis of total fatty acid composition. Furthermore, the expression of genes related to TAG accumulation; *ACX1* (Cre12.g519100) *GPD2* (Cre01.g05300) and *PGD1* (Cre03.g193500) were measured. Fig. 7A-B presents the concentration of TAG per cell for all treatments, before and after resuspension into N deplete or N replete medium. As expected, TAG concentration increases in all −N treatments, the highest increase was measured in M-24-NF cultures (62.5 fold over 6 days) and lowest in A-12-NF cultures (7 fold over 6 days). The variation of TAG content is validated with the qualitative images for Nile red fluorescence (Fig. 7C). The influence of photoperiod was more apparent in mixotrophic treatments, where initial TAG accumulation rates over the first 12 h were almost identical (0.674 and 0.671 pg $cell^{-1}$ h^{-1} for M-24-NF and M-12-NF respectively), with no significant difference ($p = 0.49$). However, between 12 and 24 h the accumulation rate continued to rise under continuous illumination, but fell during the dark period of M-12-NF treatments. Repetition of this trend is likely to have led to a reduced overall accumulation rate, and a 61% lower final TAG concentration in M-12-NF cultures (Fig. 7A-C).

The TAG accumulation response of autotrophic treatments was delayed in comparison in mixotrophic cultures. Initially, the TAG concentration in both autotrophic treatments fell slightly (although not significantly, $p > 0.05$), and then increased at a low rate in A-24-NF, but decreased further during the dark period (12 to 24 h) for A-12-NF (Fig. 7A). As demonstrated in Fig. 7B, the final mean TAG concentration of A-12-NF (2.76 pg $cell^{-1}$) was lower ($p > 0.05$) than A-24-NF (4.44 pg $cell^{-1}$), most likely due to catabolism during the dark period.

Alterations in total fatty acid composition towards saturated and monounsaturated FAs such as C16:0 and C18:1 Δ9 and away from more highly unsaturated, membrane lipid predominant FAs such as C16:4 and C18:3 Δ9,12,15, provides an indication of the change from membrane-dominated to TAG-dominated cellular lipid content [31,60]. As demonstrated in Fig. 7D, all N deprived cultures had significantly higher proportions of palmitic acid (C16:0) than the N replete control ($p < 0.001$). Interestingly both autotrophic treatments had significantly higher proportion of palmitic acid as a percentage of total lipid ($p < 0.05$) compared to mixotrophic treatments (13% higher in 24 L, 20% higher in 12 L), while proportionally more oleic acid (C18:1 Δ9) was found in the mixotrophic treatments (2.3 fold more in both 24 L and 12 L). This may indicate a preference for the prokaryotic pathway of TAG synthesis in autotrophic cultures, although determination of sn-position is needed to back up this interpretation. The proportion of C16:4 and C18:3 Δ9,12,15, found predominantly in MGDG and DGDG (diagalacterosyldiacylglycerol) [61] is highest in the control N replete treatment (11% C16:4 and 25% C18:3 Δ9,12,15). Comparatively, in both autotrophic treatments this porportion is reduced moderately (4% C16:4 and 17–18% C18:3 Δ9,12,15) but more significantly in mixotrophic treatments (1% C16:4 and 10–11% C18:3 Δ9,12,15). This trend gives an indication of the shift to TAG dominant

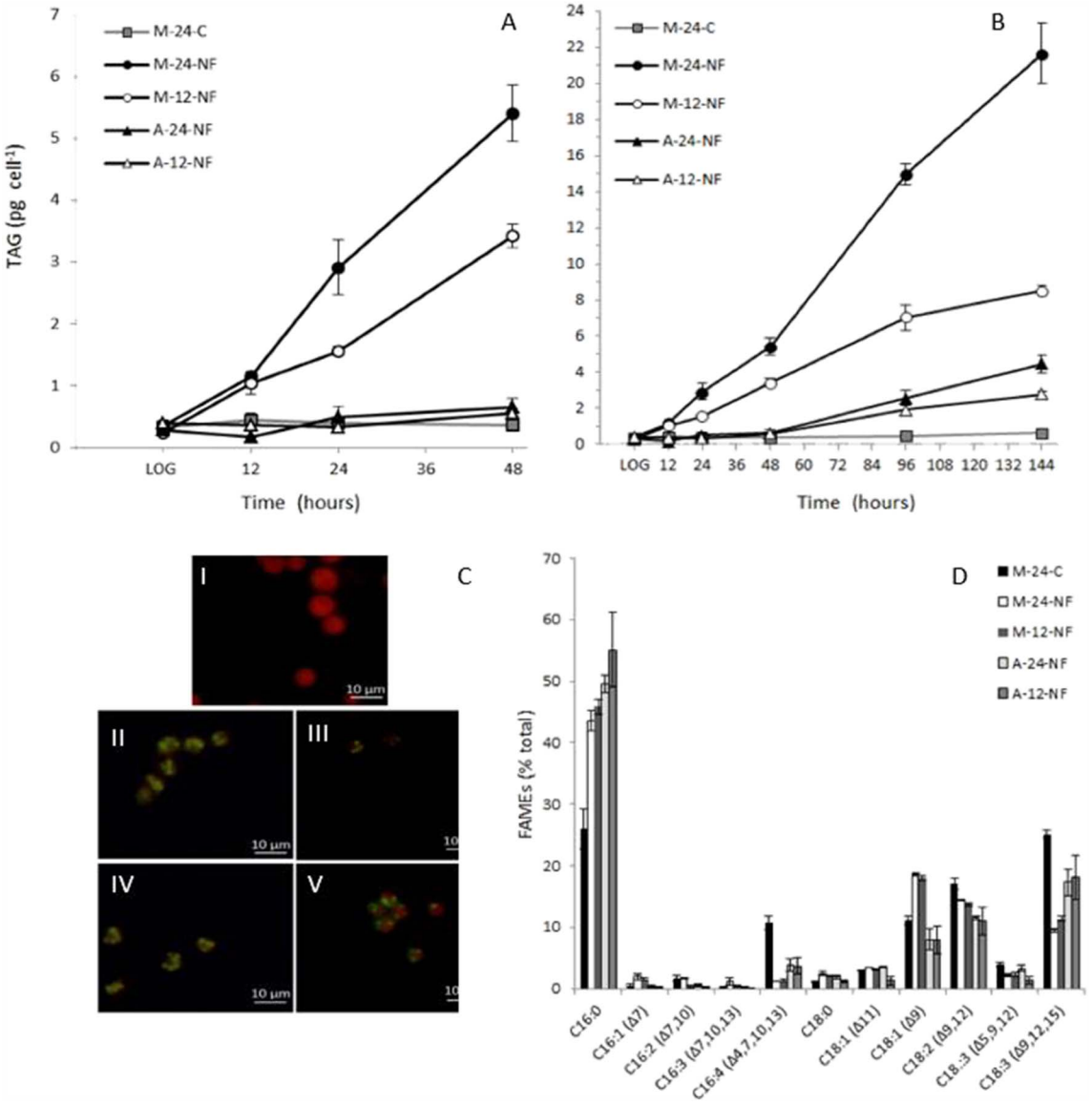

Fig. 7. A) and **B)** TAG content (pg cell^{-1}) before (LOG) and after cell resuspension in nitrogen free (NF) or replete (C) medium between **A)** 0–48 h and **B)** 0–144 h. **C)** Fluorescence microscopy of cells 144 h after resuspension in N deplete or replete (control) medium. Red fluorescence corresponds to chlorophyll autofluorescence while yellow fluorescence indicates Nile red staining of neutral lipid bodies. I) M-24-C, II) M-24-NF, III) A-24-NF, IV) M-12-NF, V) A-12-NF. **D)** Relative fatty acid composition (% of total FAMEs) 144 h after resuspension in N deplete or N replete (control) medium. Absolute quantification is presented in Fig. S1. LOG, indicates sampling point at which cells were in the log (exponential) phase of growth, immediately before transfer to N deplete (−N) medium. Treatment conditions are outlined in Table 1, M-24-C, mixotrophic continuous light, C medium; M-24-NF, mixotrophic continuous light, NF medium; M-12-NF, mixotrophic diurnal light, NF medium; A-24-NF, autotrophic continuous light, NF medium; A-12-NF, autotrophic diurnal light, NF medium. Error bars represent SE (n = 3).
Treatment conditions outlined in Table 12. Error bars represent SE (n = 3). (For interpretation of the references to colour in this figure legend, the reader is referred to the web version of this article.)

lipid profiles, although it does not provide evidence of membrane degradation as unsaturated membrane lipid FAs are typically recycled for TAG synthesis directly. There was no clear influence of photoperiod on the FA profile (Fig. 7D). Absolute quantification of FAMEs (μg per mg DCW) confirms a reduced FA accumulation in M-12-NF cultures compared to M-24-NF (43% reduction) (Fig. S1 and S2).

The gene *ACX1*, encodes the α-carboxyltransferase subunit of the plastid multimeric acetyl-CoA carboxylase enzyme, responsible for catalysing the first committal step in the FA synthesis pathway, resulting in carboxylation of acetyl-CoA to malonyl-CoA [4] (Fig. 1). Fig. 8A shows the change in *ACX1* expression over the experiment time course. N deprivation prompted a significant upregulation of *ACX1* after 2 h in all treatments ($p < 0.05$), in contrast to the initial downregulation reported for M-24-NF cultures in Goodenough et al. [12]. Similarly to *STA2* expression, for 12 h light treatments there was a dark period downregulation in *ACX1* (17.1 and 3.3 fold drop from 12 to 14 h for M-12-NF and A-12-NF respectively), however, unlike *STA2*, a significant decline ($p < 0.05$) was not recorded until after the start of the dark period (although they may have been an unrecorded peak between 2 and 12 h). A similar trend of *ACX1* upregulation was recorded in both mixotrophic and autotrophic continuous light treatments from LOG-14 h, however after a dip in expression at 24 h, M-24-NF expression increased further, peaking at 3.85 fold above average sample expression, an increase of 9.5 fold from LOG expression, while the increase in A-24-NF was more moderate (2.4 fold above average sample expression).

GPD2 is one of five genes in *C. reinhardtii* which encode NADH-dependent glycerol-3-phosphate dehydrogenase (GPDH). *GPD2* in particular is plastid targeted [12]. GPDH enables the conversion of dihydroxyacetone phosphate (DHAP) to glycerol-3-phosphate (G3P), the

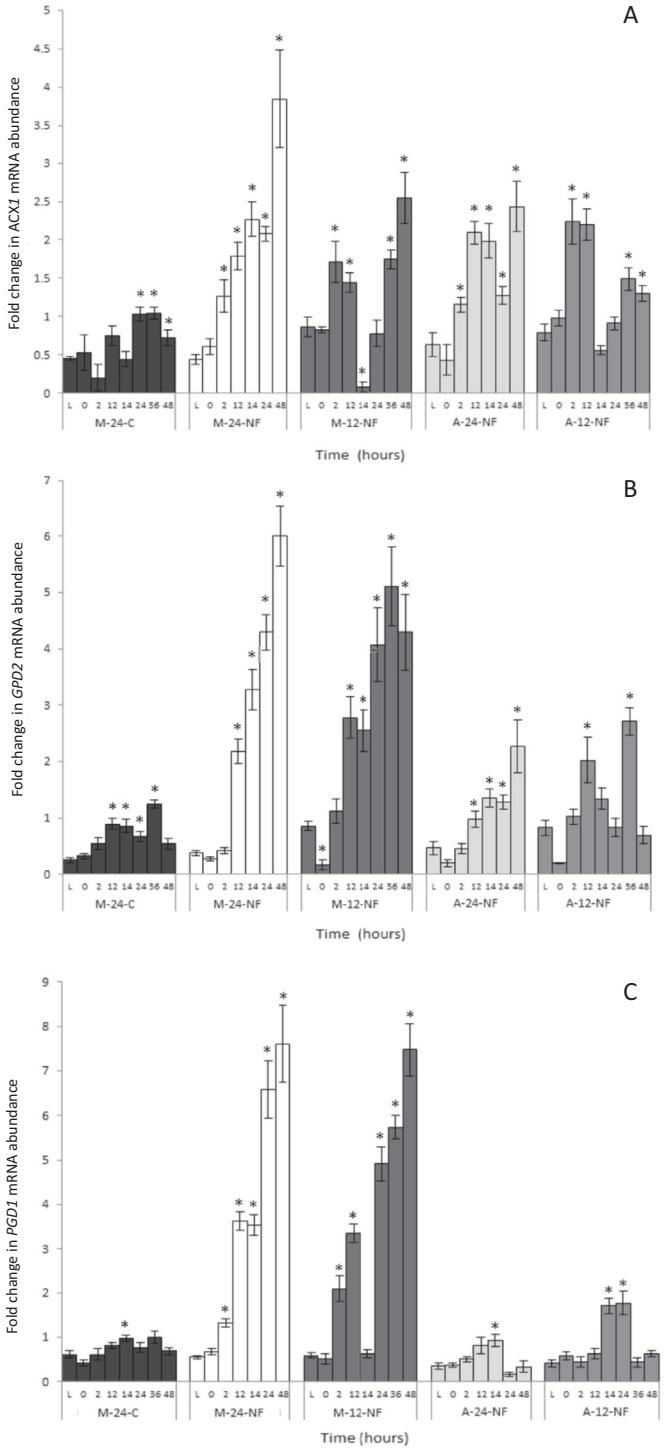

Fig. 8. Fold change (relative to the average expression of gene across all samples, time points and treatments) of **A)** *ACX1* **B)** *GPD2* **C)** *PGD1* gene expression, before (L) and after resuspension in nitrogen free (NF) or replete (C) medium. Referencing genes used for normalisation were *GAPHD, EIF1A and RCK1*. LOG, indicates sampling point at which cells were in the log (exponential) phase of growth, immediately before transfer to N deplete (−N) medium. Treatment conditions are outlined in Table 1, M-24-C, mixotrophic continuous light, C medium; M-24-NF, mixotrophic continuous light, NF medium; M-12-NF, mixotrophic diurnal light, NF medium; A-24-NF, autotrophic continuous light, NF medium; A-12-NF, autotrophic diurnal light, NF medium. Error bars represent SE ($n = 3$), * symbols indicate significant difference from L time point values (*t*-test, $p < 0.05$). For M-12-NF and A-12-NF, L(=LOG) sample taken in dark period before resuspension, then 0 to 12 h light; 12 to 24 h dark; 24 to 36 h light; 36 to 48 h dark.

backbone of glycerides such as TAG [62] (Fig. 1). DHAP is a sugar produced from the Calvin cycle and gluconeogenesis/glycolysis; consequently, the GPDH enzyme provides a major link between carbohydrate and lipid metabolism (Fig. 1). The gene *GPD2,* in particular, has been found to be highly sensitive to N deprivation in the cc-4349 strain of *C. reinhardtii*, and therefore is thought to play a major role in the TAG accumulation response [12]. The gene *GPD2* was upregulated in all −N treatments (Fig. 8B). Expression *of GPD2* also increased moderately in the nutrient replete control, although the increase in expression was comparatively small compared to N stressed treatments. There was a more pronounced influence of organic carbon addition on *GPD2* expression than *ACX1*, with both mixotrophic treatments demonstrating both a higher initial upregulation and peak expression than corresponding autotrophic treatments, with the highest mean expression found in M-24-NF after 48 h (6 fold above average sample expression), following a similar trend to that found in Goodenough et al. [12]. Organic carbon availability also altered the *GPD2* expression response to dark periods. In M-12-NF cultures at 14 h (2 h into dark period), *GLD2* expression remained stable (relative to 12 h), compared to continued upregulation in M-24-NF. In M-12-NF cultures, immediately before the start of the light period (24 h), the expression had increased (1.6 fold, relative to 14 h). In contrast, there was a drop in expression at 14 h in A-12-NF which continued to 24 h (2.4 fold drop from 12 h, $p < 0.05$). This pattern repeated over the next 24 h for the A-12-NF culture (Fig. 8B).

The gene *PGD1* (plastid galactoglycerolipid degradation 1), encodes a lipase enzyme which deacylates the predominant thylakoid membrane lipid MGDG, freeing FAs which are directed to extraplastidic lipid synthesis, particularity TAG synthesis (Fig. 1). Goodenough et al. [12] highlighted the *PGD1* encoded enzyme as a vital lipase for the conversion of pre-existing membrane lipids. Consequently, *PGD1* expression was intended in this study to provide insight into the degree of membrane degradation. However, a forward genetics study by Li et al. [31] provided evidence that *PGD1* preferentially deacylates $18{:}1^{\Delta 9}$ bound to immature MGDG which are then exported from the plastid towards TAG synthesis. The enzyme does not act on the more saturated 18:2 and 16:4 FAs found in mature MGDG (Fig. 1). Consequently, the PGD1 enzyme is not involved in mature glycoglycerolipid catabolism, but is a vital enzyme for the flux of oleic acid to the formation of TAG in *C. reinhardtii*, indeed gene deletion leads to a 50% reduction in TAG [31]. Consequently, the *PGD1* expression data provides a novel insight into potential differences in TAG biosynthesis pathways induced by different growth conditions.

As demonstrated in Fig. 8C, there was robust influence of organic carbon addition on the expression of *PGD1* in response to N deprivation. Transcript abundance in both mixotrophic treatments was significantly increased after 2 h ($p < 0.01$) and continued to increase throughout the experiment, reaching 13.8 and 12.5 fold higher expression (from LOG values) by 48 h for M-24-NF and M-12-NF respectively. In contrast, although A-24-NF experienced a transient 2.3 fold increase at 12 h (compared to log expression), the peak transcript abundance was not significantly different from the control treatment ($p > 0.05$). Photoperiod had contrasting influence on mixotrophic and autotrophic cultures, M-12-NF cultures experienced a 5.3 fold drop in expression 2 h into the dark period, which recovered at the start of the light period. Conversely, in A-12-NF treatments, the dark period correlated with a transient 2.6 fold increase ($p < 0.01$), which continued to 24 h before dropping to basal levels.

4. Discussion

4.1. Route to starch and TAG accumulation under optimal conditions

The primary aim of this study was to investigate the response of *C. reinhardtii* to N deprivation under different, and more commercially relevant, trophic and light cycle conditions. As a point of reference, it is

useful to first discuss the current understanding of the impact of N deprivation on *C. reinhardtii* under well-studied conditions of acetate supplementation and continuous light availability (M-24-NF in this study). The availability of organic carbon, specifically acetate, has been demonstrated to strongly influence the rate of TAG accumulation of *C. reinhardtii* when under N deplete conditions. While acetate is known to be an important carbon source, the uptake and flux of acetate derived carbon in *C. reinhardtii* is not fully understood. In agreement with the trend reported in previous studies (with similar conditions to M-24-NF), within the first 12 h of N deprivation, genes involved in starch metabolism are significantly upregulated [10,12], including *STA2* in this study, which had a 38-fold increase in transcript abundance over 2 h (Fig. 6B). Subsequently, carbon is diverted to starch synthesis, leading to rapid accumulation of starch, increasing 5 fold over 12 h (Fig. 6A). Beyond this point *STA2* is strongly downregulated and starch synthesis is slowed. In agreement with previous studies, genes related to TAG synthesis, particularly *GPD2* and *PGD1*, have a relatively delayed response, with upregulation starting after 2 h, and unlike *STA2*, expression continued to gradually increase over 48 h, a trend which is reflected in the continued increase of TAG [12].

Concurrently, after 24 h, *C. reinhardtii* cells grown under M-24-NF conditions suspend growth and enter an autophagy programme in which N-rich molecules mainly involved in photosynthesis and the Calvin cycle are degraded and recycled, with carbon skeletons directed to the TCA cycle or carbon storage accumulation [1,7,15]. This degradation of photosynthetic machinery leads to a greater reliance on the respiratory metabolism, as evidenced in this study by the rapid downregulation of *RBSC2* (Calvin cycle) and relative stability of *OGD1* (TCA cycle) (Fig. 4A-B). Although Calvin cycle activity is reduced, previous studies indicate that carbon sequestration continues beyond 48 h [13,17].

As noted by Goodenough et al. [12] and supported here, the degradation of photosynthetic apparatus and assumed decline in photosynthetically derived NADPH is correlated with an increase in the activity of the NADPH producing oxidative pentose phosphate pathway (*GLD2* upregulation, Fig. 4D). Alternative pathways for NAPDH production, such as malate decarboxylation by $NADP^+$ dependent malic enzyme, encoded by MME genes (*MME2, MME3, MME4, MM5, MM6*), have been reported to be stable or downregulated after N deprivation [1]. Consequently, it is likely that the oxidative phase of the PP pathway is likely to meet the increasing NADPH demand of TAG synthesis after cell chlorosis.

In agreement with previous studies [1,12], *ICL1* (encoding a key enzyme in the glyoxylate cycle) decreased significantly after 2 h and continued to decline (Fig. 4C), despite continued uptake of acetate (Fig. 4C). In a reverse genetics study, Plancke et al. [32] reported that an *ICL1* mutant, lacking a functional *ICL1* gene, accumulated 3 fold higher levels of neutral lipid compared to WT cells, and lower starch concentrations. A decline in β-oxidation proteins, but stable levels of fatty acid synthases led the authors to conclude that *ICL1* deletion resulted in TAG accumulation because of reduced lipid catabolism rather than diversion of acetyl-CoA towards FA synthesis [32]. However, this study (Fig. 7B and 8A), studies of the hyper-oleaginous *sta6* starchless mutant [10,12], and efforts to overexpress FA synthase genes [63], have all demonstrated that the gene expression or protein concentration of FA synthases does not necessarily correlate to higher FA synthesis. Alternatively, the decline in *ICL1* expression during continued acetate consumption, and rapid TAG accumulation does point to the diversion of acetate derived acetyl-CoA from production of gluconeogenic precursors (via the glyoxylate cycle) towards FA synthesis. Under N replete heterotrophic conditions, the majority of acetate derived acetyl-CoA is transported (via the peroxisome) to the mitochondria and catabolised in the TCA cycle to produce ATP [33,62]. The remaining portion is shunted through the glyoxylate cycle, involving *ICL1* (29%) or imported into the plastid (11%) [62]. This flux may not be identical in mixotrophic conditions, however the reduction in flux of the glyoxylate cycle is also likely to be correlated to a higher acetyl-CoA flux towards the TCA cycle to replace any reduction of photosynthetic flux of carbon. While this is not supported by upregulation of *OGD1*, the activity of the TCA cycle would not necessarily increase with a change in carbon source.

The response of M-24-NF cultures to N deprivation provides an important reference point for comparison with other studies and for further discussion on how the response changes when availability of carbon and light are altered.

4.2. Effect of organic carbon source

The availability of acetate has been shown to strongly influence the rate of starch and TAG accumulation of *C. reinhardtii* under N deprivation [19,20]. This trend is supported by the current study, in which M-24-NF cultures showed significant increases in the rates of starch and TAG accumulation over the first 24 h, compared to A-24-NF cultures (Fig. 7A). Despite the higher initial rate of accumulation, the peak concentration of starch was only 1.2 fold higher in M-24-NF conditions compared to A-24-NF, whereas peak TAG concentration was 6.3 fold higher. This trend supports the conclusion of Fan et al. [19] that increasing carbon availability can increase TAG accumulation, once the capacity of the dominant carbon storage compound, starch, is met. In this case acetate supplemented M-24-NF cultures rapidly peaked in starch accumulation, reaching maximum cell capacity and then diverted carbon towards TAG. In contrast starch remained the dominant carbon store for the carbon limited (no aeration) A-24-NF cultures. Davey et al. [64] reported a similar trend, in which autotrophic *C. reinhardtii*, supplied with constant CO_2 aeration reached the capacity for starch accumulation after 4–6 days, concurrent with an increased rate of TAG accumulation. TAG was reported to continue to increase over 10 days reaching a concentration 2 fold higher than the mixotrophic treatment (supplied with a finite 17.5 mM acetate supplement), highlighting the importance of exogenous carbon supply for TAG accumulation [64]. A recent radioisotope study indicated that under conditions similar to M-24-NF, 80% of carbon diverted towards starch synthesis in the first 40 h of N deprivation is derived from either photosynthetically sequestered carbon or biomass catabolism, however beyond 40 h there is a significantly increased flux of acetate derived carbon [17]. This indicates that carbon derived from acetate is likely to be diverted to the TCA cycle in the initial hours of deprivation. In carbon limited autotrophic cultures, this catabolised carbon would be sourced from inorganic sources, limiting flux towards starch synthesis.

The disparity of TAG accumulation in this study is reflected in the TAG related gene expression. As previously mentioned the trend of *ACX1* expression, involved in the first step of FA synthesis, was similar between M-24-NF and A-24-NF treatments (with the exception of the last 48 h). A similar result was reported for the related gene *BCX1* (Cre12.g484000, β-carboxyltransferase subunit of plastidic multimeric ACCase) after 2 days N deprivation [20]. A starker contrast was found in the expression of *GPD2* and *PGD1*, related to TAG rather than FA synthesis. The higher expression of plastid targeted *GPD2* in M-24-NF, indicates an increased activity of G3P production from DHAP, increasing the availability of substrate for glycerolipid synthesis (Fig. 1). The strong correlation of *GPD2* expression to TAG accumulation, unlike *ACX1*, indicates the availability of G3P may be an important bottleneck for TAG synthesis and a potential target for metabolic engineering. Finally, sustained upregulation of *PGD1* was observed in acetate supplemented cultures only. Li et al. [31] demonstrated that plastidial MGDG acts as a transient FA pool for de novo-synthesised FAs. *PGD1* is thought to enable the transfer of $18{:}1^{\Delta 9}$ (oleic acid) through the plastid membrane to cytosolic TAG lipid bodies. Consistent with this analysis, the upregulation of *PGD1* was matched by a 2.3 fold increase in $C18{:}1^{\Delta 9}$ in the total biomass FA profile (Fig. 7D). Consequently, the trend shown in Fig. 7–8 strongly indicates that the activity of PGD1, and the associated acylation of $C18{:}1^{\Delta 9}$ to TAG [31], is reliant on carbon

availability. Moreover, Lohman et al. [65] reported that increasing inorganic carbon availability had a limited impact on C18:1$^{\Delta 9}$ accumulation, indicating the observed upregulation of *PGD1* and increased C18:1$^{\Delta 9}$ found in this study is related to organic carbon availability. As *PGD1* deletion results in a 50% drop in TAG accumulation [31], the activity of this gene, and the routing of C18:1$^{\Delta 9}$ through MGDG, is likely to be an important element of the higher TAG accumulation in mixotrophic conditions. While *PGD1* is not thought to be involved in catabolism of mature MGDG, mixotrophy is likely to change the flux of C18:1$^{\Delta 9}$ destined for either extraplastidic export to TAG or further desaturation to form mature MGDG. As autotrophic cells are more reliant on a functioning photosystem it is possible *PGD1* upregulation is suppressed to retain C18:1 $^{\Delta 9}$ for further desaturation to form mature MGDG.

Further work is needed to confirm the influence of carbon availability (inorganic and organic) on *PGD1* regulation. Again, the correlation of this gene to TAG accumulation makes it a candidate target for metabolic engineering.

In this study, under N replete conditions autotrophic cultures had a higher initial chlorophyll content compared to replete mixotrophic cultures. This trend is consistent with previous research on green microalgae [53,66] and *C. reinhardtii* grown under similar conditions [64]. However, in *C. reinhardtii* the reverse trend has also been reported [67]. Polle et al. [67] recorded a 45% increase in chlorophyll content in photoheterotrophic cultures. However, the addition of bicarbonate to the mixotrophic cultures reduced the chlorophyll content back to concentrations comparable with autotrophic cultures (grown in TBP medium). The study therefore indicated that the availability of inorganic carbon impacts resource allocation to photosynthetic machinery. The flat bottle growth vessels used in [67] (as opposed to rapidly agitated flask cultures in the current study) may extenuate this trend.

As previously reported upon N deprivation, *C. reinhardtii* experienced a clear reduction in photosynthetic capacity under both mixotrophic and autotrophic cultivation [22,68]. Although autotrophic treatments had a greater rate of chlorophyll degradation over the 144 h, the slower initial reduction of chlorophyll per cell over the first 24 h compared to mixotrophic cultures led to a slower degradation of photosynthetic capacity (Fig. 3B-C) and shift towards a respiratory metabolism. This is supported by the comparatively slower downregulation of *RBSC2* and upregulation of *GLD2* and *OGD1* expression. Although after 6 days of N deprivation autotrophic cultures had a higher proportion of polyunsaturated FA (C16:4 and C18:3), typically located in galactolipids integral to the thylakoid membrane, in absolute terms the concentration of these polyunsaturated FA are lower than in mixotrophic treatments (Fig. S1). Consequently, degradation of membrane lipids cannot be directly inferred without lipidomic analysis of lipid classes.

This maintenance of photosynthetic integrity enabled autotrophic cultures to continue to channel carbon sequestered in the Calvin cycle to TAG synthesis, without compromising starch stores. In contrast the rapid photosynthetic degradation observed in mixotrophic cultures likely led to a near total reliance on acetate derived carbon for TAG synthesis and energy generation.

4.3. Effect of diurnal light and dark cycles

Circadian rhythms driven by diurnal light and dark cycles enable photosynthetic organisms to anticipate changes in energy availability in order to optimise metabolic processes and thus maximise growth [69,70]. In *C. reinhardtii* a number of physiological cycles are under diurnal control, including cell growth and division [71,72]. The major impact of light and dark cycles on cell physiology and metabolism is demonstrated at multiple levels including the transcriptome. Zones et al. [73] reported that 80% of mRNAs have significant periodic expression, including many of the genes associated with carbon metabolism. One such group of transcripts are starch related genes. Starch plays an important multifunctional role in microalgae; providing a sink for photosynthetically derived NADPH and ATP, a source of carbon for Calvin cycle intermediates, and a storage molecule to meet energy and carbon needs in the dark [22,74]. The importance of starch in *C. reinhardtii* under a diurnal light cycle is highlighted in this study by elevated expression of *STA2* and starch content at the initial N replete LOG time point, after cells had emerged from 12 h of darkness (LOG, Fig. 6A-B). In contrast, cultures grown under continuous light had negligible levels of starch in N replete conditions.

In N replete autotrophic conditions, starch is accumulated during the day when photosynthesis is active. Throughout the dark period and initial light period, in the absence of an exogenous energy and carbon source, starch is degraded and divided (during cell division) [75]. This is reflected at a transcriptome level, where starch biosynthesis genes are downregulated 2 to 3 h before the start of the dark period, then slowly upregulated during the night [73]. Under N stress; A-12-NF initially continued this diurnal cycle for at least the first light dark cycle with a simultaneous fall in both *STA2* expression and starch content. The diurnal trend in gene expression continued into the second day and starch content (sampled after dark period at 48, 96 and 144 h) while increasing, did not surpass peak levels sampled at 12 h (after light period). The transition to a respiratory dominated metabolism during the dark period was demonstrated by a transient decrease in *RBSC2* and increases in *OGD1* and *GLD2*. The strong diurnal increase in *ICL1*, despite the absence of acetate indicates the metabolism of acetyl-CoA is derived from lipid catabolism (Fig. 1). This was correlated with a decline in lipid content and downregulation of *ACX1* and *GPD2*. Unlike starch, the downregulation of genes associated with lipid metabolism did not occur until after the transition to dark. This indicates this trend is responsive and not part of a circadian rhythm. This conclusion could be tested further by carrying out a Zietgeber entrainment experiment. The evidence of catabolism at night is supported by a significantly reduced overall lipid accumulation compared to A-24-NF cultures. The reduction in TAG induced by dark periods (-36%) is a lower reduction than that observed for starch (-47%), which indicates the latter is the dominant carbon store utilised for cell maintenance in dark periods in autotrophic cells.

Interestingly in contrast to the other lipid related genes measured, the dark period induced a significant increase in *PGD1,* although it is important to note that this increase was small relative to the sustained upregulation observed in mixotrophic treatments. Transcript data reported in the supplementary data of Zones et al. [73] also showed a significant (8 fold) upregulation of *PGD1* during the dark period of autotrophic cells in N replete conditions. The upregulation of *PGD1* in both replete and deplete conditions indicates that the dark period induces a change in the flux of fatty acids in the MGDG pool. Li et al. [31] reported that mutants deficient in *PDG1* also had reduced levels of 18:1$^{\Delta 9}$ in the extraplastidic membrane betaine lipid diacylglyceryltrimethylhomoserine (DGTS) and phosphatidylethanolamine (PE). Consequently, this change in flux during the dark period may not necessarily indicate TAG synthesis but a flux of 18:1$^{\Delta 9}$ from the plastid. Given the increase in *ICL1* at this time period the flux may be towards beta-oxidation. While there may be an increase flux of FA away from mature MGDG synthesis, there was no apparent effect on maximum quantum efficiency (Fig. 3C). Clearly, the function of the important *PGD1* gene and encoded enzyme deserves further characterization.

An alternative explanation for *ICL1* dark induction in A-12-NF could be due to the availability of acetate derived from dark fermentation. During the dark period, increased respiration and absence of photosynthetic O_2 evolution could lead to hypoxic conditions. These conditions prevent oxidative phosphorylation and induce dark fermentation of starch and precursors molecules for ATP generation, producing a variety of products including acetate [76]. It is possible that this acetate is then re-assimilated via the glyoxylate pathway, inducing *ICL1* activity. However, while hypoxia occurs diurnally in natural soil

environments, or mixed population cultures, the likelihood of rapid anoxia within 2 h of darkness in low density cultures under rapid agitation is low [77]. Indeed, the transcript trend reported in this study does not correspond to a recent transcriptomic analysis of *C. reinhardtii* under anoxic conditions, which observed a decline in *OGD1* and stable levels of *ICL1* [78].

Acetate supplementation led to a very different trend of carbon accumulation under N stress. Previous studies have reported that under N replete conditions acetate supplementation extends the phase of starch accumulation, peaking 3 h into the dark period (rather than on the onset as in autotrophs) followed by a period of degradation (and cell division) [79,80]. Ral et al. [79] reported that after transfer to N free medium mixotrophic *C. reinhardtii* continue the same diurnal pattern for the first 24 h, after which cell division is suspended and the rhythm is diminished leading to a relatively stable starch concentration. In contrast, in this study, despite a continued circadian rhythm in *STA2* expression, starch in M-12-NF cultures continued to accumulate throughout the dark period. Although the accumulation rate was reduced compared to the previous 12-h light period, the 12–24 h accumulation was similar to that observed in M-24-NF conditions. Furthermore, unlike the continuous light treatment, starch continued to increase beyond 48 h, with a final concentration 49% higher than M-24-NF. Conversely, the rate of TAG accumulation (and lipid gene expression) was substantially reduced (but not halted) in M-12-NF conditions relative to M-24-NF during the dark period. This trend was correlated with a spike in *ICL1* and *OGD1,* despite reduced acetate uptake. Both the acetate assimilation pathways are reliant on ATP availability. Light stimulates acetate uptake in *Chlamydomonas* through activity of cyclic photophosphorylation [29,81,82]. This phenomenon explains the reduced rate of acetate accumulation observed in M-12-NF cultures. The diurnal light period did not have a significant impact on the rate of chlorosis or decline in F_v/F_m until beyond 96 h (Fig. 3C). The sudden decline in maximum quantum efficiency indicates that a continuous period of no photosynthetic activity during N stress may induce faster degradation of photosynthetic apparatus in mixotrophic cultures. Collectively this indicates that the loss of the remnants of photosynthetically derived carbon and energy and reduction in acetate derived acetyl-CoA during the dark period induces a switch in acetyl-CoA utilisation, away from fatty acid synthesis towards the TCA cycle and gluconeogenesis. Ultimately this response culminated in an opposite trend to that observed in autotrophic conditions, with the diurnal light period causing a substantially higher final starch content but lower TAG content.

The reasoning behind this disparity is likely to be related to the fact that starch is the dominant carbon store. In autotrophic cells, starch is accumulated and degraded in preference to TAG, while in mixotrophic cells dark periods lead to a diversion of carbon away from TAG synthesis to conserve starch accumulation. The preference for starch in cells experiencing a diurnal change in energy and carbon availability is likely to be due to the higher energy return on investment. Starch synthesis consumes approximately 49 ATP equivalents (eq), while degradation generates 32 ATP eq. (65.3%). In comparison fatty acid synthesis (palmitic acid) consumes 171 ATP eq and produces 108 ATP eq through degradation (60.5%) [29]. This higher efficiency makes starch a more suitable energy store for diurnal cycling and is a possible reason for the initial preference of starch accumulation in all treatments. As a result, in N stressed conditions *C. reinhardtii* cells under diurnal circadian rhythm have a metabolic preference for starch storage. Conversely while TAG is a less efficient storage compound, it is considerably more energy dense (2.45 fold) than starch [83], and consequently is preferential for longer term storage once the cellular capacity for starch is met.

5. Conclusion

In conclusion, this study demonstrates that both carbon availability and photoperiod have a strong influence on the metabolic response of *C. reinhardtii* to N deprivation. Acetate supplementation leads to faster photosynthetic degradation and a rapid shift towards a respiratory dominant metabolism. Once the capacity of starch storage is met, acetate is funnelled towards the synthesis of TAG, leading to significantly higher lipid accumulation. Of particular note is the apparent reliance on acetate availability for the upregulation of *PGD1,* correlated with an increase in oleic acid ($C18:1^{\Delta 9}$) in the FA profile; a phenomenon which requires further investigation. Diurnal dark periods resulted in a rapid reduction in carbon accumulation in both mixotrophic and autotrophic conditions. Without acetate supplementation both starch and lipid are catabolised at night, while in mixotrophic cultures lipid synthesis is suspended in preference to continued starch accumulation. Ultimately both trends are informative for both commercial production and metabolic targeting. The significant impact of both photoperiod and carbon availability on the central carbon metabolism is likely to impact the efficacy of metabolic engineering. Therefore, the impact of genetic modifications should be investigated under both mixotrophic and autotrophic conditions, and particularly under both continuous light and more commercially relevant photoperiod conditions.

Acknowledgements

The research was funded by the Engineering and Physical Sciences Research Council (EPSRC) (grant number EP/G037477/1) and carried out as part of the E Futures DTC at the University of Sheffield. Authors would like to thank Taylor Weiss (currently at Arizona State University, USA) and Simon Thorpe (currently at University of Sheffield, UK) for useful technical discussions.

Declaration of author contribution

R.T.S and D.J.G conceived the research and designed the experiments; R.S performed the experiments, analysed and interpreted the data. R.T.S wrote the article. R.S and D.J.G supervised and edited the manuscript. R.T.S and D.J.G read and approved the final manuscript. R.T.S (richard.smith@rothamsted.ac.uk) and D.J.G (d.j.gilmour@rothamsted.ac.uk) take responsibility for the integrity of the research and manuscript.

R.T.S - Richard T Smith.

D.J.G - D. Jim Gilmour.

Conflict of interests

The authors declare that they have no conflicts of interest.

Statement of informed consent, human/animal rights

No conflicts, informed consent, human or animal rights applicable.

Appendix A. Supplementary data

Supplementary data to this article can be found online at https://doi.org/10.1016/j.algal.2018.01.020.

References

[1] S. Schmollinger, T. Mühlhaus, N.R. Boyle, I.K. Blaby, D. Casero, T. Mettler, J.L. Moseley, J. Kropat, F. Sommer, D. Strenkert, D. Hemme, M. Pellegrini, A.R. Grossman, M. Stitt, M. Schroda, S.S. Merchant, Nitrogen-sparing mechanisms in *Chlamydomonas* affect the transcriptome, the proteome, and photosynthetic metabolism, Plant Cell 26 (2014) 1410–1435, http://dx.doi.org/10.1105/tpc.113.122523.

[2] S.S. Merchant, J. Kropat, B. Liu, J. Shaw, J. Warakanont, TAG, You're it! *Chlamydomonas* as a reference organism for understanding algal triacylglycerol accumulation, Curr. Opin. Biotechnol. 23 (2012) 352–363, http://dx.doi.org/10.1016/j.copbio.2011.12.001.

[3] D. Lopez, D. Casero, S.J. Cokus, S.S. Merchant, M. Pellegrini, Algal functional

annotation tool: a web-based analysis suite to functionally interpret large gene lists using integrated annotation and expression data, BMC Bioinf. 12 (2011) 282, http://dx.doi.org/10.1186/1471-2105-12-282.

[4] S.S. Merchant, S.E. Prochnik, O. Vallon, E.H. Harris, S.J. Karpowicz, G.B. Witman, A. Terry, A. Salamov, L.K. Fritz-Laylin, L. Maréchal-Drouard, W.F. Marshall, L.-H. Qu, D.R. Nelson, A.A. Sanderfoot, M.H. Spalding, V.V. Kapitonov, Q. Ren, P. Ferris, E. Lindquist, H. Shapiro, S.M. Lucas, J. Grimwood, J. Schmutz, P. Cardol, H. Cerutti, G. Chanfreau, C.-L. Chen, V. Cognat, M.T. Croft, R. Dent, S. Dutcher, E. Fernández, H. Fukuzawa, D. González-Ballester, D. González-Halphen, A. Hallmann, M. Hanikenne, M. Hippler, W. Inwood, K. Jabbari, M. Kalanon, R. Kuras, P.A. Lefebvre, S.D. Lemaire, A.V. Lobanov, M. Lohr, A. Manuell, I. Meier, L. Mets, M. Mittag, T. Mittelmeier, J.V. Moroney, J. Moseley, C. Napoli, A.M. Nedelcu, K. Niyogi, S.V. Novoselov, I.T. Paulsen, G. Pazour, S. Purton, J.-P. Ral, D.M. Riaño-Pachón, W. Riekhof, L. Rymarquis, M. Schroda, D. Stern, J. Umen, R. Willows, N. Wilson, S.L. Zimmer, J. Allmer, J. Balk, K. Bisova, C.-J. Chen, M. Elias, K. Gendler, C. Hauser, M.R. Lamb, H. Ledford, J.C. Long, J. Minagawa, M.D. Page, J. Pan, W. Pootakham, S. Roje, A. Rose, E. Stahlberg, A.M. Terauchi, P. Yang, S. Ball, C. Bowler, C.L. Dieckmann, V.N. Gladyshev, P. Green, R. Jorgensen, S. Mayfield, B. Mueller-Roeber, S. Rajamani, R.T. Sayre, P. Brokstein, I. Dubchak, D. Goodstein, L. Hornick, Y.W. Huang, J. Jhaveri, Y. Luo, D. Martínez, W.C.A. Ngau, B. Otillar, A. Poliakov, A. Porter, L. Szajkowski, G. Werner, K. Zhou, I.V. Grigoriev, D.S. Rokhsar, A.R. Grossman, The *Chlamydomonas* genome reveals the evolution of key animal and plant functions, Science 318 (2007) 245–250, http://dx.doi.org/10.1126/science.1143609.

[5] D. González-Ballester, D. Casero, S. Cokus, M. Pellegrini, S.S. Merchant, A.R. Grossman, RNA-Seq analysis of sulfur-deprived *Chlamydomonas* cells reveals aspects of acclimation critical for cell survival, Plant Cell 22 (2010) 2058–2084, http://dx.doi.org/10.1105/tpc.109.071167.

[6] R. Miller, G. Wu, R.R. Deshpande, A. Vieler, K. Gärtner, X. Li, E.R. Moellering, S. Zäuner, A.J. Cornish, B. Liu, B. Bullard, B.B. Sears, M.-H. Kuo, E.L. Hegg, Y. Shachar-Hill, S.-H. Shiu, C. Benning, Changes in transcript abundance in *Chlamydomonas reinhardtii* following nitrogen deprivation predict diversion of metabolism, Plant Physiol. 154 (2010) 1737–1752, http://dx.doi.org/10.1104/pp.110.165159.

[7] J. Longworth, J. Noirel, J. Pandhal, P.C. Wright, S. Vaidyanathan, HILIC- and SCX-based quantitative proteomics of *Chlamydomonas reinhardtii* during nitrogen starvation induced lipid and carbohydrate accumulation, J. Proteome Res. 11 (2012) 5959–5971, http://dx.doi.org/10.1021/pr300692t.

[8] E.R. Moellering, C. Benning, RNA interference silencing of a major lipid droplet protein affects lipid droplet size in *Chlamydomonas reinhardtii*, Eukaryot. Cell 9 (2010) 97–106, http://dx.doi.org/10.1128/EC.00203-09.

[9] D.Y. Lee, J.-J. Park, D.K. Barupal, O. Fiehn, System response of metabolic networks in *Chlamydomonas reinhardtii* to total available ammonium, Mol. Cell. Proteomics 11 (2012) 973–988, http://dx.doi.org/10.1074/mcp.M111.016733.

[10] I.K. Blaby, A.G. Glaesener, T. Mettler, S.T. Fitz-Gibbon, S.D. Gallaher, B. Liu, N.R. Boyle, J. Kropat, M. Stitt, S. Johnson, C. Benning, M. Pellegrini, D. Casero, S.S. Merchant, Systems-level analysis of nitrogen starvation–induced modifications of carbon metabolism in a *Chlamydomonas reinhardtii* starchless mutant, Plant Cell 25 (2013) 4305–4323, http://dx.doi.org/10.1105/tpc.113.117580.

[11] N.R. Boyle, M.D. Page, B. Liu, I.K. Blaby, D. Casero, J. Kropat, S. Cokus, A. Hong-Hermesdorf, J. Shaw, S.J. Karpowicz, S. Gallaher, S. Johnson, C. Benning, M. Pellegrini, A. Grossman, S.S. Merchant, Three acyltransferases and a nitrogen responsive regulator are implicated in nitrogen starvation-induced triacylglycerol accumulation in *Chlamydomonas*, J. Biol. Chem. 287 (2012) 15811–15825, http://dx.doi.org/10.1074/jbc.M111.334052.

[12] U. Goodenough, I. Blaby, D. Casero, S.D. Gallaher, C. Goodson, S. Johnson, J.-H. Lee, S.S. Merchant, M. Pellegrini, R. Roth, J. Rusch, M. Singh, J.G. Umen, T.L. Weiss, T. Wulan, The path to triacylglyceride obesity in the sta6 strain of *Chlamydomonas reinhardtii*, Eukaryot. Cell 13 (2014) 591–613, http://dx.doi.org/10.1128/EC.00013-14.

[13] M.T. Juergens, R.R. Deshpande, B.F. Lucker, J.-J. Park, H. Wang, M. Gargouri, F.O. Holguin, B. Disbrow, T. Schaub, J.N. Skepper, D.M. Kramer, D.R. Gang, L.M. Hicks, Y. Shachar-Hill, The regulation of photosynthetic structure and function during nitrogen deprivation in *Chlamydomonas reinhardtii*, Plant Physiol. 167 (2015) 558–573, http://dx.doi.org/10.1104/pp.114.250530.

[14] J.-J. Park, H. Wang, M. Gargouri, R.R. Deshpande, J.N. Skepper, F.O. Holguin, M.T. Juergens, Y. Shachar-Hill, L.M. Hicks, D.R. Gang, The response of *Chlamydomonas reinhardtii* to nitrogen deprivation: a systems biology analysis, Plant J. 81 (2015) 611–624, http://dx.doi.org/10.1111/tpj.12747.

[15] N. Wase, P.N. Black, B.A. Stanley, C.C. DiRusso, Integrated quantitative analysis of nitrogen stress response in *Chlamydomonas reinhardtii* using metabolite and protein profiling, J. Proteome Res. 13 (2014) 1373–1396, http://dx.doi.org/10.1021/pr400952z.

[16] F.G. Plumley, G.W. Schmidt, Nitrogen-dependent regulation of photosynthetic gene expression, Proc. Natl. Acad. Sci. U. S. A. 86 (1989) 2678–2682.

[17] M.T. Juergens, B. Disbrow, Y. Shachar-Hill, The relationship of triacylglycerol and starch accumulation to carbon and energy flows during nutrient deprivation in *Chlamydomonas reinhardtii*, Plant Physiol. 171 (2016) 2445–2457, http://dx.doi.org/10.1104/pp.16.00761.

[18] M.H. Spalding, Chapter 8 - the CO2-concentrating mechanism and carbon assimilation, in: E.H. Harris, D.B. Stern, G.B. Witman (Eds.), The *Chlamydomonas* Sourcebook, Second Edition, Academic Press, London, 2009, pp. 257–301, , http://dx.doi.org/10.1016/B978-0-12-370873-1.00016-2.

[19] J. Fan, C. Yan, C. Andre, J. Shanklin, J. Schwender, C. Xu, Oil accumulation is controlled by carbon precursor supply for fatty acid synthesis in *Chlamydomonas reinhardtii*, Plant Cell Physiol. 53 (2012) 1380–1390, http://dx.doi.org/10.1093/pcp/pcs082.

[20] B.-H. Kim Ramanan, D.-H. Cho, S.-R. Ko, H.-M. Oh, H.-S. Kim, Lipid droplet synthesis is limited by acetate availability in starchless mutant of *Chlamydomonas reinhardtii*, FEBS Lett. 587 (2013) 370–377, http://dx.doi.org/10.1016/j.febslet.2012.12.020.

[21] Y. Li, D. Han, G. Hu, D. Dauvillee, M. Sommerfeld, S. Ball, Q. Hu, *Chlamydomonas* starchless mutant defective in ADP-glucose pyrophosphorylase hyper-accumulates triacylglycerol, Metab. Eng. 12 (2010) 387–391, http://dx.doi.org/10.1016/j.ymben.2010.02.002.

[22] Y. Li, D. Han, G. Hu, M. Sommerfeld, Q. Hu, Inhibition of starch synthesis results in overproduction of lipids in *Chlamydomonas reinhardtii*, Biotechnol. Bioeng. 107 (2010) 258–268, http://dx.doi.org/10.1002/bit.22807.

[23] Z.T. Wang, N. Ullrich, S. Joo, S. Waffenschmidt, U. Goodenough, Algal lipid bodies: stress induction, purification, and biochemical characterization in wild-type and Starchless *Chlamydomonas reinhardtii*, Eukaryot. Cell 8 (2009) 1856–1868, http://dx.doi.org/10.1128/EC.00272-09.

[24] Y. Chisti, Biodiesel from microalgae, Biotechnol. Adv. 25 (2007) 294–306, http://dx.doi.org/10.1016/j.biotechadv.2007.02.001.

[25] Q. Hu, M. Sommerfeld, E. Jarvis, M. Ghirardi, M. Posewitz, M. Seibert, A. Darzins, Microalgal triacylglycerols as feedstocks for biofuel production: perspectives and advances, Plant J. 54 (2008) 621–639, http://dx.doi.org/10.1111/j.1365-313X.2008.03492.x.

[26] R.H. Wijffels, M.J. Barbosa, An outlook on microalgal biofuels, Science 329 (2010) 796–799, http://dx.doi.org/10.1126/science.1189003.

[27] A. Baker, D.J. Carrier, T. Schaedler, H.R. Waterham, C.W. van Roermund, F.L. Theodoulou, Peroxisomal ABC transporters: functions and mechanism, Biochem. Soc. Trans. 43 (2015) 959–965, http://dx.doi.org/10.1042/BST20150127.

[28] C. Andre, J.E. Froehlich, M.R. Moll, C. Benning, A Heteromeric Plastidic pyruvate kinase complex involved in seed oil biosynthesis in Arabidopsis, Plant Cell 19 (2007) 2006–2022, http://dx.doi.org/10.1105/tpc.106.048629.

[29] X. Johnson, J. Alric, Central carbon metabolism and electron transport in *Chlamydomonas reinhardtii*: metabolic constraints for carbon partitioning between oil and starch, Eukaryot. Cell 12 (2013) 776–793, http://dx.doi.org/10.1128/EC.00318-12.

[30] Y. Li-Beisson, F. Beisson, W. Riekhof, Metabolism of acyl-lipids in *Chlamydomonas reinhardtii*, Plant J. 82 (2015) 504–522, http://dx.doi.org/10.1111/tpj.12787.

[31] X. Li, E.R. Moellering, B. Liu, C. Johnny, M. Fedewa, B.B. Sears, M.-H. Kuo, C. Benning, A Galactoglycerolipid lipase is required for triacylglycerol accumulation and survival following nitrogen deprivation in *Chlamydomonas reinhardtii*, Plant Cell 24 (2012) 4670–4686, http://dx.doi.org/10.1105/tpc.112.105106.

[32] C. Plancke, H. Vigeolas, R. Höhner, S. Roberty, B. Emonds-Alt, V. Larosa, R. Willamme, F. Duby, D. Onga Dhali, P. Thonart, S. Hiligsmann, F. Franck, G. Eppe, P. Cardol, M. Hippler, C. Remacle, Lack of isocitrate lyase in *Chlamydomonas* leads to changes in carbon metabolism and in the response to oxidative stress under mixotrophic growth, Plant J. 77 (2014) 404–417, http://dx.doi.org/10.1111/tpj.12392.

[33] K. Yoon, D. Han, Y. Li, M. Sommerfeld, Q. Hu, Phospholipid:diacylglycerol acyltransferase is a multifunctional enzyme involved in membrane lipid turnover and degradation while synthesizing triacylglycerol in the unicellular green microalga *Chlamydomonas reinhardtii*, Plant Cell 24 (2012) 3708–3724, http://dx.doi.org/10.1105/tpc.112.100701.

[34] F. Kong, Y. Liang, B. Légeret, A. Beyly-Adriano, S. Blangy, R.P. Haslam, J.A. Napier, F. Beisson, G. Peltier, Y. Li-Beisson, *Chlamydomonas* carries out fatty acid β-oxidation in ancestral peroxisomes using a bona fide acyl-CoA oxidase, Plant J. 90 (2017) 358–371, http://dx.doi.org/10.1111/tpj.13498.

[35] Y. Li, D. Han, K. Yoon, S. Zhu, M. Sommerfeld, Q. Hu, Molecular and cellular mechanisms for lipid synthesis and accumulation in microalgae: biotechnological implications, in: A. Richmond, Q. Hu (Eds.), Handbook of Microalgal Culture, John Wiley & Sons, Ltd, 2013, pp. 545–565.

[36] K.J. Lauersen, R. Willamme, N. Coosemans, M. Joris, O. Kruse, C. Remacle, Peroxisomal microbodies are at the crossroads of acetate assimilation in the green microalga *Chlamydomonas reinhardtii*, Algal Res. 16 (2016) 266–274, http://dx.doi.org/10.1016/j.algal.2016.03.026.

[37] Y. Kan, J. Pan, A one-shot solution to bacterial and fungal contamination in the green alga *Chlamydomonas reinhardtii* culture by using an antibiotic Cocktail1, J. Phycol. 46 (2010) 1356–1358, http://dx.doi.org/10.1111/j.1529-8817.2010.00904.x.

[38] N. Sueoka, Mitotic replication of deoxyribonucleic acid in *Chlamydomonas reinhardi*, PNAS 46 (1960) 83–91.

[39] A.A. Mendes, P.C. Oliveira, H.F. de Castro, Properties and biotechnological applications of porcine pancreatic lipase, J. Mol. Catal. B Enzym. 78 (2012) 119–134, http://dx.doi.org/10.1016/j.molcatb.2012.03.004.

[40] S. Van Wychen, L.M.L. Laurens, Determination of Total Lipids as Fatty Acid Methyl Esters (FAME) by in situ Transesterfication, National Renewable Energy Laboratory, Golden, CO, USA, 2013.

[41] L.M.L. Laurens, M. Quinn, S. Van Wychen, D.W. Templeton, E.J. Wolfrum, Accurate and reliable quantification of total microalgal fuel potential as fatty acid methyl esters by in situ transesterification, Anal. Bioanal. Chem. 403 (2012) 167–178, http://dx.doi.org/10.1007/s00216-012-5814-0.

[42] W. Chen, M. Sommerfeld, Q. Hu, Microwave-assisted Nile red method for in vivo quantification of neutral lipids in microalgae, Bioresour. Technol. 102 (2011) 135–141, http://dx.doi.org/10.1016/j.biortech.2010.06.076.

[43] L.M.L. Laurens, S. Van Wychen, J.P. McAllister, S. Arrowsmith, T.A. Dempster, J. McGowen, P.T. Pienkos, Strain, biochemistry, and cultivation-dependent measurement variability of algal biomass composition, Anal. Biochem. 452 (2014)

86–95, http://dx.doi.org/10.1016/j.ab.2014.02.009.
[44] L.M.L. Laurens, T.A. Dempster, H.D.T. Jones, E.J. Wolfrum, S. Van Wychen, J.S.P. McAllister, M. Rencenberger, K.J. Parchert, L.M. Gloe, Algal biomass constituent analysis: method uncertainties and investigation of the underlying measuring chemistries, Anal. Chem. 84 (2012) 1879–1887, http://dx.doi.org/10.1021/ac202668c.
[45] S. Jeffrey, G. Humphrey, New spectrophotometric equations for determining chlorophylls a, b, c1 and c2 in higher plants, algae and natural populations, Biochem. Physiol. Pflanz. 167 (1975) 191–194.
[46] U. Schreiber, P. Quayle, S. Schmidt, B.I. Escher, J.F. Mueller, Methodology and evaluation of a highly sensitive algae toxicity test based on multiwell chlorophyll fluorescence imaging, Biosens. Bioelectron. 22 (2007) 2554–2563, http://dx.doi.org/10.1016/j.bios.2006.10.018.
[47] S.A. Bustin, J.-F. Beaulieu, J. Huggett, R. Jaggi, F.S. Kibenge, P.A. Olsvik, L.C. Penning, S. Toegel, MIQE précis: practical implementation of minimum standard guidelines for fluorescence-based quantitative real-time PCR experiments, BMC Mol. Biol. 11 (2010) 74, http://dx.doi.org/10.1186/1471-2199-11-74.
[48] B. Thornton, C. Basu, Real-time PCR (qPCR) primer design using free online software, Biochem. Mol. Biol. Educ. 39 (2011) 145–154, http://dx.doi.org/10.1002/bmb.20461.
[49] S. Arvidsson, M. Kwasniewski, D.M. Riaño-Pachón, B. Mueller-Roeber, QuantPrime – a flexible tool for reliable high-throughput primer design for quantitative PCR, BMC Bioinformatics. 9 (2008) 465, http://dx.doi.org/10.1186/1471-2105-9-465.
[50] J.M. Gallup, M.R. Ackermann, Addressing fluorogenic real-time qPCR inhibition using the novel custom excel file system "FocusField2-6GallupqPCRSet-upTool-001" to attain consistently high fidelity qPCR reactions, Biol Proced Online. 8 (2006) 87–152, http://dx.doi.org/10.1251/bpo122.
[51] C.L. Andersen, J.L. Jensen, T.F. Ørntoft, Normalization of real-time quantitative reverse transcription-PCR data: a model-based variance estimation approach to identify genes suited for normalization, applied to bladder and colon cancer data sets, Cancer Res. 64 (2004) 5245–5250, http://dx.doi.org/10.1158/0008-5472.CAN-04-0496.
[52] J. Hellemans, G. Mortier, A.D. Paepe, F. Speleman, J. Vandesompele, qBase relative quantification framework and software for management and automated analysis of real-time quantitative PCR data, Genome Biol. 8 (2007) R19, http://dx.doi.org/10.1186/gb-2007-8-2-r19.
[53] R.T. Smith, K. Bangert, S.J. Wilkinson, D.J. Gilmour, Synergistic carbon metabolism in a fast growing mixotrophic freshwater microalgal species Micractinium inermum, Biomass Bioenergy 82 (2015) 73–86, http://dx.doi.org/10.1016/j.biombioe.2015.04.023.
[54] T.F. Gallagher, R.J. Ellis, Light-stimulated transcription of genes for two chloroplast polypeptides in isolated pea leaf nuclei, EMBO J. 1 (1982) 1493–1498, http://dx.doi.org/10.1002/j.1460-2075.1982.tb01345.x.
[55] M.L. Pilgrim, C.R. McClung, Differential involvement of the circadian clock in the expression of genes required for ribulose-1,5-bisphosphate carboxylase/oxygenase synthesis, assembly, and activation in *Arabidopsis thaliana*, Plant Physiol. 103 (1993) 553–564.
[56] M.F. Dunn, J.A. Ramírez-Trujillo, I. Hernández-Lucas, Major roles of isocitrate lyase and malate synthase in bacterial and fungal pathogenesis, Microbiology 155 (2009) 3166–3175, http://dx.doi.org/10.1099/mic.0.030858-0.
[57] B. Delrue, T. Fontaine, F. Routier, A. Decq, J.M. Wieruszeski, N.V.D. Koornhuyse, M.L. Maddelein, B. Fournet, S. Ball, Waxy *Chlamydomonas reinhardtii*: monocellular algal mutants defective in amylose biosynthesis and granule-bound starch synthase activity accumulate a structurally modified amylopectin, J. Bacteriol. 174 (1992) 3612–3620.
[58] M.L. Maddelein, N. Libessart, F. Bellanger, B. Delrue, C. D'Hulst, N.V. den Koornhuyse, T. Fontaine, J.M. Wieruszeski, A. Decq, S. Ball, Toward an understanding of the biogenesis of the starch granule. Determination of granule-bound and soluble starch synthase functions in amylopectin synthesis, J. Biol. Chem. 269 (1994) 25150–25157.
[59] F. Wattebled, A. Buléon, B. Bouchet, J.-P. Ral, L. Liénard, D. Delvallé, K. Binderup, D. Dauvillée, S. Ball, C. D'Hulst, Granule-bound starch synthase I, Eur. J. Biochem. 269 (2002) 3810–3820, http://dx.doi.org/10.1046/j.1432-1033.2002.03072.x.
[60] G.O. James, C.H. Hocart, W. Hillier, H. Chen, F. Kordbacheh, G.D. Price, M.A. Djordjevic, Fatty acid profiling of *Chlamydomonas reinhardtii* under nitrogen deprivation, Bioresour. Technol. 102 (2011) 3343–3351, http://dx.doi.org/10.1016/j.biortech.2010.11.051.
[61] H.M. Nguyen, M. Baudet, S. Cuiné, J.-M. Adriano, D. Barthe, E. Billon, C. Bruley, F. Beisson, G. Peltier, M. Ferro, Y. Li-Beisson, Proteomic profiling of oil bodies isolated from the unicellular green microalga *Chlamydomonas reinhardtii*: with focus on proteins involved in lipid metabolism, Proteomics 11 (2011) 4266–4273, http://dx.doi.org/10.1002/pmic.201100114.
[62] G. Klöck, K. Kreuzberg, Kinetic properties of asn-glycerol-3-phosphate dehydrogenase purified from the unicellular alga *Chlamydomonas reinhardtii*, Biochim. Biophys. Acta Gen. Subj. 991 (1989) 347–352, http://dx.doi.org/10.1016/0304-4165(89)90127-X.
[63] R. Radakovits, R.E. Jinkerson, A. Darzins, M.C. Posewitz, Genetic engineering of algae for enhanced biofuel production, Eukaryot. Cell 9 (2010) 486–501, http://dx.doi.org/10.1128/EC.00364-09.
[64] P.T. Davey, W.C. Hiscox, B.F. Lucker, J.V. O'Fallon, S. Chen, G.L. Helms, Rapid triacylglyceride detection and quantification in live micro-algal cultures via liquid state ^{1}H NMR, Algal Res. 1 (2012) 166–175, http://dx.doi.org/10.1016/j.algal.2012.07.003.
[65] E.J. Lohman, R.D. Gardner, L.D. Halverson, B.M. Peyton, R. Gerlach, Carbon partitioning in lipids synthesized by *Chlamydomonas reinhardtii* when cultured under three unique inorganic carbon regimes, Algal Res. 5 (2014) 171–180, http://dx.doi.org/10.1016/j.algal.2014.08.001.
[66] B. Cheirsilp, S. Torpee, Enhanced growth and lipid production of microalgae under mixotrophic culture condition: effect of light intensity, glucose concentration and fed-batch cultivation, Bioresour. Technol. 110 (2012) 510–516, http://dx.doi.org/10.1016/j.biortech.2012.01.125.
[67] J.E.W. Polle, J.R. Benemann, A. Tanaka, A. Melis, Photosynthetic apparatus organization and function in the wild type and a chlorophyll b-less mutant of *Chlamydomonas reinhardtii*. Dependence on carbon source, Planta 211 (2000) 335–344, http://dx.doi.org/10.1007/s004250000279.
[68] J. Msanne, D. Xu, A.R. Konda, J.A. Casas-Mollano, T. Awada, E.B. Cahoon, H. Cerutti, Metabolic and gene expression changes triggered by nitrogen deprivation in the photoautotrophically grown microalgae *Chlamydomonas reinhardtii* and *Coccomyxa* sp. C-169, Phytochemistry 75 (2012) 50–59, http://dx.doi.org/10.1016/j.phytochem.2011.12.007.
[69] Y. Niwa, T. Matsuo, K. Onai, D. Kato, M. Tachikawa, M. Ishiura, Phase-resetting mechanism of the circadian clock in *Chlamydomonas reinhardtii*, PNAS 110 (2013) 13666–13671, http://dx.doi.org/10.1073/pnas.1220004110.
[70] Z.B. Noordally, A.J. Millar, Clocks in algae, Biochemistry 54 (2015) 171–183, http://dx.doi.org/10.1021/bi501089x.
[71] F.R. Cross, J.G. Umen, The *Chlamydomonas* cell cycle, Plant J. 82 (2015) 370–392, http://dx.doi.org/10.1111/tpj.12795.
[72] M. Mittag, S. Kiaulehn, C.H. Johnson, The circadian clock in *Chlamydomonas reinhardtii*. What is it for? What is it similar to? Plant Physiol. 137 (2005) 399–409, http://dx.doi.org/10.1104/pp.104.052415.
[73] J.M. Zones, I.K. Blaby, S.S. Merchant, J.G. Umen, High-resolution profiling of a synchronized diurnal transcriptome from *Chlamydomonas reinhardtii* reveals continuous cell and metabolic differentiation, Plant Cell 27 (2015) 2743–2769, http://dx.doi.org/10.1105/tpc.15.00498.
[74] A. Krishnan, G.K. Kumaraswamy, D.J. Vinyard, H. Gu, G. Ananyev, M.C. Posewitz, G.C. Dismukes, Metabolic and photosynthetic consequences of blocking starch biosynthesis in the green alga *Chlamydomonas reinhardtii* sta6 mutant, Plant J. 81 (2015) 947–960, http://dx.doi.org/10.1111/tpj.12783.
[75] C. Thyssen, R. Schlichting, C. Giersch, The CO2-concentrating mechanism in the physiological context: lowering the CO2 supply diminishes culture growth and economises starch utilisation in *Chlamydomonas reinhardtii*, Planta 213 (2001) 629–639, http://dx.doi.org/10.1007/s004250100534.
[76] C.P. Catalanotti, W. Yang, M.C. Posewitz, A.R. Grossman, Fermentation metabolism and its evolution in algae, Front. Plant Sci. 4 (2013), http://dx.doi.org/10.3389/fpls.2013.00150.
[77] W. Yang, C. Catalanotti, T.M. Wittkopp, M.C. Posewitz, A.R. Grossman, Algae after dark: mechanisms to cope with anoxic/hypoxic conditions, Plant J. 82 (2015) 481–503, http://dx.doi.org/10.1111/tpj.12823.
[78] A. Hemschemeier, D. Casero, B. Liu, C. Benning, M. Pellegrini, T. Happe, S.S. Merchant, COPPER RESPONSE REGULATOR1–dependent and –independent responses of the *Chlamydomonas reinhardtii* transcriptome to dark anoxia[W], Plant Cell 25 (2013) 3186–3211, http://dx.doi.org/10.1105/tpc.113.115741.
[79] J.-P. Ral, C. Colleoni, F. Wattebled, D. Dauvillée, C. Nempont, P. Deschamps, Z. Li, M.K. Morell, R. Chibbar, S. Purton, C. d'Hulst, S.G. Ball, Circadian clock regulation of starch metabolism establishes GBSSI as a major contributor to amylopectin synthesis in *Chlamydomonas reinhardtii*, Plant Physiol. 142 (2006) 305–317, http://dx.doi.org/10.1104/pp.106.081885.
[80] R. Willamme, Z. Alsafra, R. Arumugam, G. Eppe, F. Remacle, R.D. Levine, C. Remacle, Metabolomic analysis of the green microalga *Chlamydomonas reinhardtii* cultivated under day/night conditions, J. Biotechnol. 215 (2015) 20–26, http://dx.doi.org/10.1016/j.jbiotec.2015.04.013.
[81] M. Gibbs, R.P. Gfeller, C. Chen, Fermentative metabolism of *Chlamydomonas reinhardii* III. Photoassimilation of acetate, Plant Physiol. 82 (1986) 160–166, http://dx.doi.org/10.1104/pp.82.1.160.
[82] R.W. Eppley, R. Gee, P. Saltman, Photometabolism of acetate by *Chlamydomonas mundana*, Physiol. Plant. 16 (1963) 777–792, http://dx.doi.org/10.1111/j.1399-3054.1963.tb08355.x.
[83] S. Subramanian, A.N. Barry, S. Pieris, R.T. Sayre, Comparative energetics and kinetics of autotrophic lipid and starch metabolism in chlorophytic microalgae: implications for biomass and biofuel production, Biotechnol. Biofuels 6 (2013) 150, http://dx.doi.org/10.1186/1754-6834-6-150.